Malate-dependent Fe accumulation is a critical checkpoint in the root developmental response to low phosphate

Javier Mora-Macías*[a], Jonathan Odilón Ojeda-Rivera*[a], Dolores Gutiérrez-Alanís[a], Lenin Yong-Villalobos[a], Araceli Oropeza-Aburto[a], Javier Raya González[a], Gabriel Jiménez-Domínguez[a], Gabriela Chávez-Calvillo[a], Rubén Rellán-Álvarez[a] and Luis Herrera-Estrella[a1]

*These authors contributed equally to this work.

[1]To whom correspondence should be addressed: lherreae@cinvestav.mx

Author affiliations:

[a]Laboratorio Nacional de Genómica para la Biodiversidad (Langebio)/Unidad de Genómica Avanzada, Centro de Investigación y Estudios Avanzados del Instituto Politécnico Nacional, 36500 Irapuato, Guanajuato, México;

Abstract

Low phosphate (Pi) availability constrains plant development and crop production in both natural and agricultural ecosystems. When Pi is scarce, modifications of root system architecture (RSA) enhance soil exploration ability and can lead to an increase in Pi uptake. In *Arabidopsis*, an iron-dependent determinate developmental program that induces premature differentiation in the root apical meristem (RAM) begins when the root tip contacts low Pi media, resulting in a short-root phenotype. However, the mechanisms that enable the regulation of root growth in response to Pi-limiting conditions remain largely unknown. Cellular, genomic and transcriptomic analysis of low-Pi insensitive mutants revealed that the malate-exudation related genes *SENSITIVE TO PROTON RHIZOTOXICITY* (*STOP1*) and *ALUMINUM ACTIVATED MALATE TRANSPORTER 1* (*ALMT1*) represent a critical checkpoint in the root developmental response to Pi starvation in *Arabidopsis thaliana*.

Introduction

Phosphorus is an essential nutrient for plant development, a constituent of key molecules such as nucleic acids, ATP and membrane phospholipids. Plants take up and metabolize phosphorus in the inorganic form of orthophosphate (Pi) (1). Pi is the least accessible macronutrient in many natural and agricultural ecosystems and its low availability in the soil often limits plant growth and productivity. Under phosphate limiting conditions (-Pi), plants activate an array of genetic (2–6), biochemical (7, 8) and morphological modifications (9–11) that enhance their ability to cope with low Pi availability.

Arabidopsis responses to low Pi availability have been divided in systemic responses that depend upon the internal Pi status of the plant and local responses that depend upon the level of Pi available in the external medium (5, 12). A molecular dissection of local and systemic responses to Pi starvation using transcriptomic analysis has been reported (5). Systemic responses include the up-regulation of genes involved in the overall enhancement of Pi uptake and Pi internal use efficiency, and are largely controlled by the master regulator PHR1 (a Myb transcription factor) (6, 13). Local responses include alterations of root traits such as the inhibition of primary root growth (14), an increase in lateral root density (10) and higher density and length of root hairs (9). These changes in root system architecture have been proposed to enhance the soil exploration ability of the plant by increasing root surface area of exploration in the top layers of the soil where Pi tends to accumulate. Some evidence indicates that there is some degree of crosstalk between local and systemic responses to low Pi availability as mutants altered in root system architecture responses to low Pi also have an altered expression of genes involved in systemic responses (15).

Growth of *Arabidopsis* seedlings under *in vitro* Pi-limiting conditions induces a determinate developmental program known as RAM exhaustion (11). RAM exhaustion consists of the loss of meristematic potential and the arrest of cell

2

63 proliferation, leading to the inhibition of primary root growth. Meristematic potential
64 is lost due to premature differentiation of the cells that constitute the stem cell niche
65 (SCN), which includes the quiescent center (QC). Cell proliferation in the RAM is
66 lost due to a gradual reduction in mitotic activity. Root-tip contact with low
67 phosphate media (16) in the presence of iron (17) has been reported as essential
68 for the inhibition of primary root growth in response to Pi deficiency conditions in
69 *Arabidopsis thaliana*. *Arabidopsis* mutants that fail to trigger root system
70 morphological responses to low Pi have been reported previously (15, 16). Two of
71 these mutants, *low phosphate root 1* and *2* (*lpr1 and lpr2*) were found to be
72 affected in genes encoding multicopper oxidases, suggesting that a metal with
73 different levels of oxidation could be involved in the alteration of root system
74 architecture in response to low Pi availability (16). A mutant that is hypersensitive
75 to low Pi, *phosphate deficiency response 2* (*pdr2*), and triggers the root system
76 response to low Pi availability faster that the wild-type (WT) was also reported (18).
77 *PDR2* encodes an ER localized P_5-type ATPase (19). *PDR2* and *LPR1* have been
78 proposed to orchestrate RAM-exhaustion in a genetically interacting route under
79 low Pi conditions (19). Whilst the precise function of *PDR2* has not been
80 determined, LPR1 is essential for primary root inhibition under low Pi conditions
81 and it has been shown to have ferroxidase activity (16, 19, 20). An LPR1-
82 dependent accumulation of Fe^{3+} in the apoplast of cells in the elongation and
83 meristematic regions of the primary root, that triggers the production of reactive
84 oxygen species (ROS), is essential for meristem exhaustion in low-Pi media (20).
85 ROS generation correlates with callose deposition in the RAM, which was
86 proposed to activate meristem exhaustion by blocking the cell-to-cell movement of
87 SHORT-ROOT (SHR), a transcription factor that is essential for stem cell
88 maintenance in the RAM (20). However, the mechanism that regulates iron
89 accumulation and relocation in the RAM remains largely unknown.

90

91   In this work, we characterized two *low phosphate insensitive* mutants (*lpi5*
92 *and lpi6*), which, in contrast to the short root phenotype of WT *Arabidopsis*
93 seedlings, show normal primary root elongation in low Pi media. Mapping by

94   sequencing revealed that the *lpi5* corresponds to *SENSITIVE TO PROTON*

95   *RHIZOTOXICITY (STOP1)* and *lpi6* to *ALUMINUM ACTIVATED MALATE*

96   *TRANSPORTER 1* (*ALMT1),* the two genes previously reported to be responsible

97   for activating malate efflux in the roots of Arabidopsis seedlings exposed to toxic

98   concentrations of aluminum (21–23). Genetic, cellular and transcriptomic analysis

99   shows that *STOP1* and *ALMT1* are required for a malate-dependent accumulation

100   of iron in the root meristem, which leads to alterations in the redox balance that

101   triggers primary root growth inhibition and RAM exhaustion in response to Pi

102   deficiency conditions in *Arabidopsis thaliana*.

103

104   **Results**

105

106   ***Arabidopsis* EMS-mutants *lpi5* and *lpi6* show indeterminate primary**

107   **root growth under phosphate deficiency conditions**

108

109   The *Arabidopsis thaliana* Col-0 accession seedlings grown in media

110   containing low Pi concentrations (below 50 µM Pi) show a short root phenotype

111   defined by a determinate pattern of primary root growth and RAM differentiation. To

112   identify mutants that are insensitive to the effect of low Pi on primary root growth,

113   we screened an EMS-mutagenized Col-0 population for mutant lines presenting a

114   long root phenotype under low-Pi (-Pi, 5 µM Pi) conditions. We isolated

115   approximately 50 mutant lines with different alterations in the primary root growth in

116   response to low-Pi availability. Two lines that were insensitive to the effect of low Pi

117   on primary root growth, which we named *low phosphorus insensitive 5 and low*

118   *phosphorus insensitive 6* (*lpi5* and *lpi6*), were chosen for further characterization

119   (Figure 1A, B, C). When grown under high Pi (+Pi; 100µM Pi) conditions, both *lpi5*

120   and *lpi6* seedlings presented a primary root length similar to the WT *Arabidopsis*

121   Col-0 accession (Figure 1A). Under -Pi conditions at 10 dag, WT plants had a

122   visible reduction in primary root growth, whereas *lpi5* and *lpi6* seedlings had

123   primary root elongation similar to that of WT seedlings grown in +Pi media which is

124   four-fold longer than that of Pi-deprived WT seedlings (Figure 1B). Although *lpi5*

125 seedlings had a long root phenotype in –Pi media, they had a slightly shorter

126 primary root than the WT and *lpi6* in +Pi media and were also slightly shorter than

127 *lpi6* in -Pi medium (Figure 1A, C). Analysis of segregation frequencies under -Pi

128 conditions showed that the long root phenotype in *lpi5 and lpi6* is the result of

129 single recessive mutations (Supplementary Table 1).

130

131 In Pi-deprived *Arabidopsis* seedlings, the short-root phenotype is

132 accompanied by a reduction in cell proliferation and meristematic activity during the

133 process of RAM exhaustion (11). To test for signs of RAM exhaustion in *lpi5* and

134 *lpi6* seedlings grown in –Pi media, we examined the expression of the

135 *proCycB1::GUS* cell cycle activity marker (24) and the *proQC46::GUS* quiescent

136 center (QC) identity marker (25). In +Pi media, WT, *lpi5* and *lpi6* seedlings showed

137 clear cell proliferation activity as indicated by the *proCycB1::GUS* signal and an

138 active QC as shown by the *proQC46::GUS* signal (Figure 1D). In -Pi media at 10

139 dag the cell cycle and QC marker genes were undetectable in WT seedlings,

140 whereas GUS staining was clearly detectable for both the cell cycle

141 (*proCycB1::GUS*) and QC (*proQC46::GUS*) markers in the primary root of *lpi5* and

142 *lpi6* (Figure 1D). These results show that, in contrast to the WT, low Pi does not

143 trigger meristem exhaustion in the RAM of *lpi5* and *lpi6* seedlings.

144

145

146

147
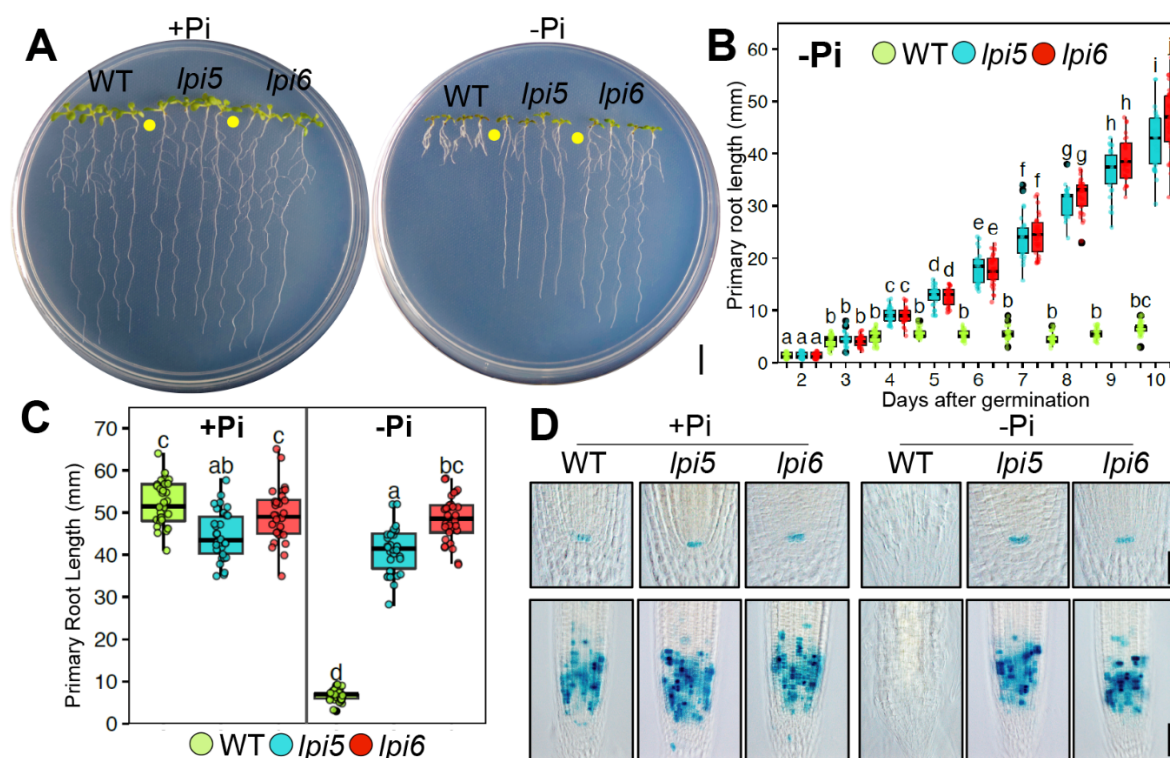
Figure 1. Low-Pi insensitive mutants continue primary root growth and RAM maintenance under Pi deficiency conditions. (A) Phenotypes of WT, lpi5 and lpi6 seedlings grown under high (100 μM Pi; +Pi) and low Pi (5 μM Pi; -Pi) conditions 10 days-after-germination (dag). Scale bar equals 1 centimeter (cm). (B) Primary root growth kinetics of seedlings grown under -Pi conditions from 2 to 10 dag. Green, blue and red dots depict WT, *lpi5* and *lpi6* individuals (n=30 from 3 independent experiments), respectively. Statistical groups were determined using a Tukey HSD test (P-value < .05) and are indicated with letters. (C) Primary root length of seedlings grown under +Pi and -Pi conditions. Green, blue and red dots depict WT, lpi5 and lpi6 individuals (n=30 from 3 independent experiments), respectively. Statistical groups were determined using a Tukey HSD test (P-value < .05) and are indicated with letters. (D) GUS staining of *proCycB1::GUS* and *proQC46::GUS* expression in the RAM of WT, *lpi5* and *lpi6* seedlings 10 dag. Scale bar indicates 100 μm.

lpi5 and _lpi6_ have mutations in the transcription factor _STOP1_ and the malate transporter _ALMT1,_ respectively.


We used a mapping-by-sequencing approach to identify the genes responsible for the *lpi5* and *lpi6* phenotypes (See Materials and Methods). We identified 12 and 18 specific homozygous variants (missense, frameshift and

168   splice-donor) potentially linked to *lpi5* and *lpi6* mutant phenotypes, respectively.

169   Given the alterations of primary root of *lpi5* and *lpi6* seedlings in response to an

170   environmental stress, we focused on the homozygous mutations that could

171   potentially be linked to alterations in root morphological or root responses to abiotic

172   stress. Among the potential candidates responsible for the root phenotype of *lpi5*

173   and *lpi6* under low Pi conditions, *SENSITIVE TO PROTON RHIZOTOXICITY*

174   *(STOP1)* and *ALUMINUM ACTIVATED MALATE TRANSPORTER 1 (ALMT1)* were

175   particularly interesting because both genes have been previously reported to

176   participate in the tolerance of the *Arabidopsis* root to toxic concentrations of Al^{+3}.

177   *STOP1 (*At1g34370) encodes a zinc finger protein transcription factor that plays a

178   critical role in Al^{3+} tolerance and acid soil tolerance in *Arabidopsis* (21). *ALMT1*

179   encodes a transmembrane protein that mediates malate efflux in the root in

180   response to the presence of toxic Al^{3+} levels (22), and its expression has been

181   shown to be activated by *STOP1* in response to Al stress conditions (21).

182

183   To test whether the long root phenotype of *lpi5, lpi6* was indeed due to

184   lesions in STOP1 and ALMT1, we tested the phenotype of T-DNA insertional

185   mutants in *STOP1 (SALK_114108)* and *ALMT1 (SALK_009629)* in –Pi and +Pi

186   media. In +Pi media, WT, *lpi6* and *almt1* seedlings had a similar primary root

187   length, whereas *lpi5* and *stop1* had a slightly shorter root length than the WT

188   (Figure 2A-B). In -Pi media, the T-DNA insertional mutants *stop1* and *almt1* had a

189   long root phenotype that contrasted with the short root phenotype of the WT

190   (Figure 2A-B). It has been reported that *stop1* is sensitive to low pH (4.7) and

191   levels of Al^{3+} (2 μM) that are not yet toxic for *Arabidopsis* WT seedlings and that

192   *almt1* is also sensitive to this Al^{3+} concentration (28). We also found that *lpi5* was

193   sensitive to low pH and Al (as is *stop1)* and that *lpi6* was sensitive to Al but not to

194   low pH (as observed for *almt1)* (Supplementary Figure 1). Crosses between *lpi5*

195   and *almt1,* and between *lpi6* and *stop1*, showed that *lpi5* and *lpi6* are mutant

196   alleles of *STOP1* and *ALMT1*, respectively (Supplementary Figure 1).

197

198

199   Mapping-by-sequencing of *lpi5* revealed a C:T (CAT:TAT) substitution in the

200   +84 position of *STOP1*. *In silico* analysis predicted that the *lpi5* mutation caused an

201   amino acid substitution (H168Y) that replaces one of the two histidine residues that

202   are crucial for the formation of first of the four zinc fingers of the DNA binding

203   domain of STOP1 (Figure 2C). The first zinc finger domain of STOP1 is critical to

204   bind to the promoter of its target genes (29). Mapping-by-sequencing of the *lpi6*

205   mutant revealed a 13-base-pair deletion in the first exon of *ALMT1* starting at

206   position +757 (Figure 2D). *In silico* analysis predicted that this deletion causes a

207   frameshift mutation that produces an aberrant protein that lacks 200 amino-acids of

208   the carboxy-terminal moiety of ALMT1 (Figure 2D). Our *in silico* sequence analysis

209   further confirmed that *lpi5* and *lpi6* are EMS-induced mutant alleles of *STOP1* and

210   *ALMT1*, respectively.

211
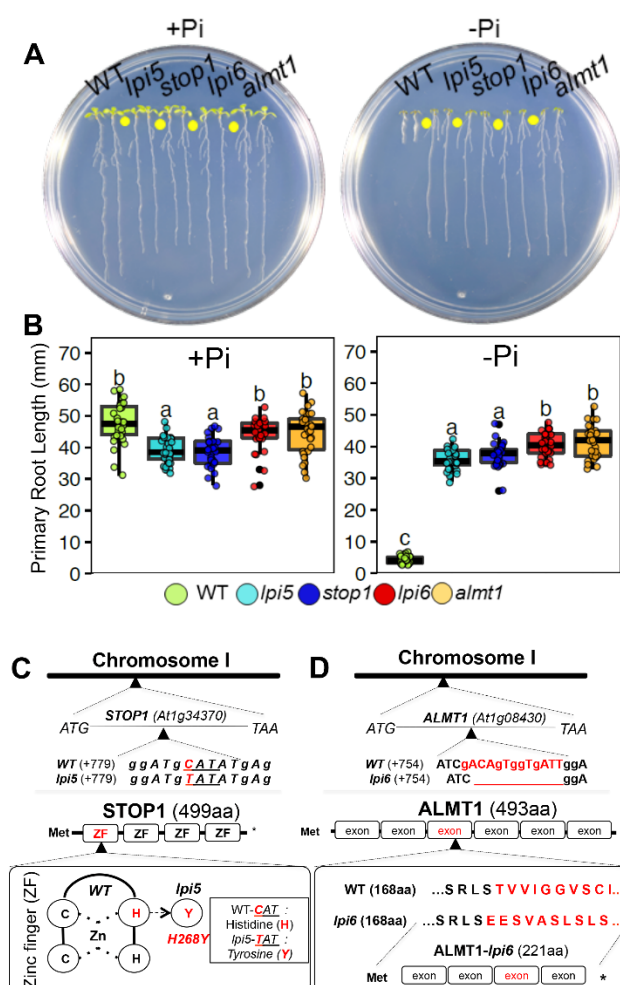
Figure 2. Mapping by sequencing revealed *lpi5* and *lpi6* to be *stop1* and *almt1* mutants, respectively. (A) Phenotypes of Col-0, *lpi5, stop1, almt1* and *lpi6* seedlings grown under high phosphate (+Pi) and low phosphate (-Pi) conditions 10 dag. (B) Primary root length of WT, *lpi5, stop1, almt1* and *lpi6* seedlings grown under high phosphate (+Pi) or low phosphate (-Pi) conditions 10 dag. Dots depict WT, *lpi5, stop1, almt1* and *lpi6* individuals (n=30 from 3 independent experiments). Statistical groups were determined using a Tukey HSD test (P-value < .05) and are indicated with letters. (A) C:T (CAT : TAT) substitution in the +84 base within the At1g34370 locus of the *lpi5* genome. *lpi5* mutation causes an amino acid substitution (H168Y) that replaces one of the two histidine residues of the four zinc fingers that constitute STOP1 (B) 13 base pair deletion in the +757 base pair position within the first exon of the At1g08430 locus of the *lpi6* genome. The 13 base deletion present in *lpi6* causes a frameshift mutation that produces an aberrant protein with 200 amino-acids less than the WT.

ALMT1 is expressed in the RAM of *Arabidopsis* under Pi deficiency conditions before meristematic exhaustion

To determine whether the expression of *STOP1* and *ALMT1* is regulated by Pi availability in the root tip, we analyzed the expression of *STOP1* and *ALMT1* in the root apex of 5 dag WT and *stop1* seedlings using qRT-PCR (Figure 3A, Supplementary Figure 3). In the WT, *ALMT1* expression increased by approximately 4-fold in response to -Pi conditions, while the level of expression of *STOP1* was not significantly altered by Pi availability (Figure 3A). We also found that in the *stop1* background the expression of *ALMT1* was undetectable (Supplementary Figure 2). Our results confirm a previous report (21) showing that *STOP1* is essential for the expression of *ALMT1*, but also show that *STOP1* is required for the induction of *ALMT1* in response to low Pi.

Since *STOP1* and *ALMT1* appear to be essential for RAM-exhaustion under Pi deficiency conditions*,* we examined the cell-specific expression pattern of these two genes in seedlings grown under +Pi and -Pi conditions 5 dag, a time point prior to full RAM exhaustion (Figure 1C), but when primary root growth inhibition has already started (Figure 1C). Confocal microscopy of *proSTOP1::GUS::GFP* seedlings grown in +Pi media revealed that *STOP1* is expressed in the QC, columella, lateral root cap and epidermis (Figure 3B) and that its expression

245   pattern is not altered in –Pi media (Figure 3B). On the other hand no detectable

246   reporter activity of *proALMT1::GUS::GFP* was found in the RAM of seedlings

247   grown under +Pi conditions, whereas in –Pi media expression of the reporter gene

248   was clearly detectable in the proximal region of the SCN (QC, cortex and stele

249   initials), vascular bundle, pericycle, cortex, endodermis, columella and lateral root

250   cap (Figure 3B).

251
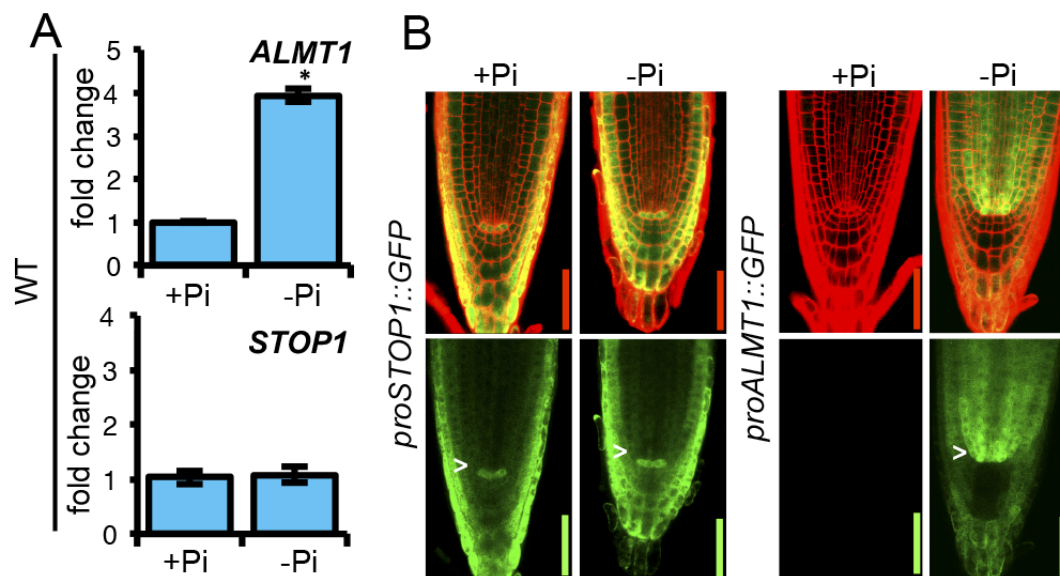
252   **Figure 3. *STOP1* and *ALMT1* are expressed in the RAM of *Arabidopsis* under Pi**

253   **deficiency conditions.** (A) qRT-PCR analysis of *STOP1* and *ALMT1* expression in the root apex

254   (2-3 mm) of WT (Col-0) plants. Bars represent the mean fold change ±SEM of 2 biological

255   replicates with 3 technical replicates. WT +Pi samples were used as calibrator values. *ACT2* and

256   *UBQ10* were used as internal controls. Asterisk indicates that the expression was significantly

257   different between +Pi and –Pi conditions (Student t-test; $p < 0.05$) (B) Transgenic Col-0 plants

258   harboring transcriptional gene fusions containing the *STOP1* and *ALMT1* promoter fused to a

259   double GFP-GUS reporter gene, respectively (*proSTOP1::GUS::GFP* and *proALMT1::GUS::GFP)*,

260   were grown under +Pi and -Pi conditions and expression activity was observed at 5 dag using

261   confocal microscopy. Scale bar indicates 100 µm.

262

263   **Malate treatment rescues the determinate developmental program in**

264   **the primary root of *stop1* and *almt1* in response to low Pi conditions**

265

266   Since malate efflux has been shown to be affected in *stop1* and *almt1*

267   mutants and both *stop1* and *almt1* present determinate primary root growth under

10

268 Al^{3+} toxicity conditions (21, 22), we sought to determine whether malate exudation

269 also played a role in the *Arabidopsis* primary root response to low Pi availability. To

270 this end, we added increasing concentrations of malate to both +Pi and -Pi media

271 and tested the effect of malate treatment on the primary root growth of WT, *stop1*

272 and *almt1* seedlings (Figure 4 and Supplementary Figure 3). We observed that

273 primary root growth was not altered by malate treatment under +Pi conditions in

274 any of the tested lines (Supplementary Figure 3). However, in -Pi media, treatment

275 with malate restored the short-root phenotype in *stop1* and *almt1* seedlings in a

276 concentration-dependent manner (Figure 4A-B). Although *stop1* seedlings treated

277 with 1 mM malate had significantly shorter roots than in media lacking malate, their

278 primary roots were slightly, but statistically significantly, larger than those of the WT

279 and *almt1* seedlings grown in the same media (Figure 4A-B). Malate treatment of

280 Pi-deprived WT seedlings showed a small effect at 0.1 mM, however, this effect

281 was not observed at higher malate concentrations (Figure 4A-B) as WT seedlings

282 remained short under all treatments (Figure 4A).

283

284 To determine whether malate treatment activates RAM exhaustion in *stop1*

285 and *almt1* seedlings, we examined the expression of *proCycB1::GUS* and

286 *proQC46::GUS* reporter genes in Pi-deprived/malate-treated *stop1* and *almt1*

287 seedlings. Clear signs of cell differentiation in the RAM of Pi-deprived/malate-

288 treated *almt1* seedlings were observed and *proCycB1::GUS* and *proQC46::GUS*

289 reporter activity was undetectable. In the case of Pi-deprived/malate-treated *stop1*

290 seedlings, although cell proliferation was reduced, it was not completely arrested

291 and *proQC46::GUS* expression was still clearly detectable (Figure 4C). No

292 expression was found in the WT either in low-Pi media or low-Pi media

293 supplemented with 1 mM malate (Figure 4C).
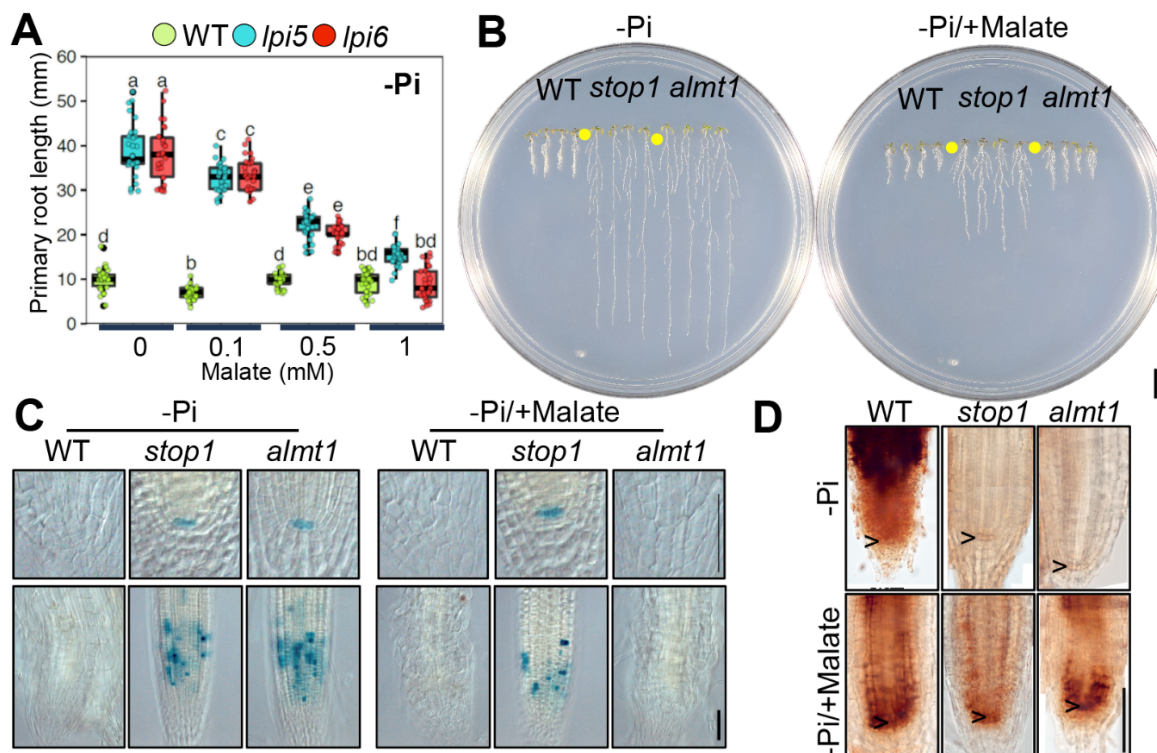
Figure 4. Malate treatment rescues the mutant phenotype of *stop1* and *almt1* seedlings. (A) Primary root length of 10 dag WT, *stop1* and *almt1* seedlings grown under increasing concentration of malate supplemented to -Pi medium. Green, blue and red dots depict WT, *stop1* and *almt1* individuals (n=30 from 3 independent experiments), respectively. Statistical groups were determined using Tukey HSD test (P-value <.05) and are indicated with letters. (B) Phenotypes of 10 dag WT, *stop1* and *almt1* seedlings grown under low phosphate medium (-Pi) and low phosphate medium supplemented with 1mM malate (-Pi/+Malate). Scale bar equals 1 mm. (C) *proCycB1::GUS* (lower panels) and *proQC46::GUS* (upper panels) expression (D) Perls-DAB iron staining in the RAM of WT, *stop1* and *almt1* grown under -Pi and malate treatment (1 mM; –Pi/+Malate) conditions 5 dag. Scale bar equals 100 µm.

Fe accumulation is absent in the RAM of Pi-deprived *stop1* and *almt1* seedlings and can be rescued by malate treatment

Accumulation of Fe in the apoplast of cells in the RAM is required to activate the primary root response to low Pi availability (20). As carboxylate-iron complexes have been reported to participate in iron transport and acquisition in plants (30–32) and malate efflux is affected in *stop1* and *almt1* mutants (21, 22), we explored whether malate exudation plays a role in the Fe accumulation mechanism that is

314   required to trigger primary root growth inhibition in response to low Pi availability.

315   First, we tested whether malate is required for the accumulation of Fe in the

316   apoplast of RAM cells using Perls-DAB histochemical Fe staining, which allows the

317   detection of changes in labile Fe^{3+} [20], on the root tips of WT, *stop1* and *almt1* in

318   low Pi media with or without 1 mM malate (Figure 4D and Supplementary Figure

319   3). In Pi-deprived seedlings not exposed to malate, Fe staining was clearly

320   observed in the roots of WT seedlings while *stop1* and *almt1* seedlings showed a

321   much lower Fe accumulation (Figure 4D). In Pi-deprived WT seedlings treated with

322   1 mM malate, Fe staining was still clearly visible but in a more defined zone of the

323   root apex, which included the QC. In contrast to *stop1* and *almt1* seedlings grown

324   in -Pi media lacking malate, those treated with 1 mM of this organic acid showed a

325   very similar pattern to that observed for the WT under the same conditions.

326   Although malate-treated Pi-deprived *stop1* seedlings show a clear Fe staining,

327   accumulation of Fe^{3+} in the RAM was apparently lower around the QC than that

328   observed for the WT and *almt1* seedlings treated with malate (Figure 4C). We did

329   not observe significant differences in the patterns of Fe staining between the root

330   tips of WT, *stop1* and *almt1* seedlings under +Pi conditions treated with 1 mM

331   malate (Supplementary Figure 3).

332

333   Citrate, as well as malate, is an organic acid that is released by plant roots

334   in response to low-Pi availability [33]. Since organic acids are naturally occurring

335   metal chelating agents, and if the malate chelating-effect is responsible for the

336   primary root growth inhibition in -Pi media, we wanted to test whether citrate

337   treatment of Pi-deprived seedlings (1 mM citrate) could also phenocopy the short-

338   root phenotype in Pi-deprived *stop1* and *almt1* seedlings. In –Pi media, we

339   observed that citrate treatment slightly reduced primary root elongation of *stop1*

340   seedlings (10%) (Supplementary Figure 4A-B) and had no significant effect in the

341   root growth of Pi-deprived *almt1* seedlings (Supplementary Figure 4A-B).

342   Interestingly, citrate treatment of Pi-deprived WT seedlings resulted in an average

343   2.5 fold increase in root length compared to that observed for WT seedlings grown

344   in low-Pi media in the absence of citrate (Supplementary Figure 4A-B). These

345   results suggest a specific role of malate in primary root growth inhibition by
346   promoting the accumulation of Fe in the apoplast of root cells in the meristematic
347   area.

348

349   As malate is capable of inducing root growth inhibition and meristem
350   exhaustion in *almt1* seedlings, linked to an effect on Fe-accumulation in the RAM
351   of *almt1* seedlings, we hypothesized that malate has a chelating effect on Fe that
352   contributes to its accumulation in the root tip. To test our hypothesis, we performed
353   molecular dynamic calculations to simulate the effect of malate on the aggregation
354   of metallic ions such as Fe^{2+}, Fe^{3+} and Al^{3+}. We built 4 different simulation sets
355   using ascending malate:metal molecular ratios, starting from 0:120 to 120:120
356   (Supplementary Figure 5). We observed non-bonded interactions between malate
357   and Fe^{2+} ions but the interactions did not induce Fe^{2+} aggregation in any of the
358   simulated systems (Supplementary Figure 5). In the case of the malate and Fe^{3+}
359   system we observed non-bonded interactions and the formation of large malate-
360   Fe^{3+} aggregates in all ratios tested with an increasing size of aggregates when an
361   equimolar concentration of malate and Fe^{3+} was used (Supplementary Figure 5).
362   Metals did not aggregate when malate was not included in the simulation set
363   (Supplementary Figure 5). These results suggest that malate can form large
364   aggregates with Fe^{3+} and Al^{3+} but not with Fe^{2+}, which could be relevant for the
365   activation of the *Arabidopsis* primary root response to low Pi.

366

367   **Differential expression analysis revealed a preferential loss of local**
368   **transcriptional responses to Pi starvation in *stop1* and *almt1* root tips**

369

370   The root tip plays a fundamental role in the ability of the root system to
371   sense and respond to Pi starvation (16). Therefore, to understand the role of
372   *STOP1* and *ALMT1* in the local and systemic responses of the *Arabidopsis* root to
373   low phosphate, we performed a whole transcriptome sequencing (RNA-seq)
374   analysis of gene expression in root tips from WT, *stop1* and *almt1* seedlings grown

375   under +Pi and -Pi conditions (Figure 5). We performed pairwise comparisons of

376   transcript abundances between -Pi and +Pi conditions to determine differentially

377   expressed genes (-1.5 < logFC < 1.5; FDR<.05) in response to Pi deficiency in WT,

378   *stop1* and *almt1* root tips (Figure 5A). A total of 1488 genes were found to be

379   responsive to low phosphate in the WT (819 up; 669 down), while only 569 in

380   *stop1* (294 up; 275 down) and 463 in *almt1* (224 up; 239 down) (Figure 5A). To

381   identify the biological processes whose expression is misregulated in the root apex

382   of *stop1* and *almt1* in response to Pi availability, we performed a Gene Ontology

383   (GO) enrichment analysis (Figure 5). First, we performed a GO clusterization of all

384   the over-represented categories that included genes that belong to the same

385   biological process in the root tips of WT seedlings (Figure 5B). We found seven

386   clusters that were named after the most significantly over-represented category of

387   the cluster and included the cellular response to phosphate starvation

388   (GO:0016036), secondary metabolism (GO:0019748), macromolecule metabolic

389   process (GO:0044260), cell wall organization (GO:0071555) and systemic

390   acquired resistance (GO:0009627). A full list of the GO categories that were

391   enriched in the WT is included in Supplementary File 1. We then performed an

392   analysis of the percentage of genes belonging to each cluster that were

393   differentially expressed in *stop1* and *almt1* relative to the WT (Figure 5C). Using

394   such an approach we determined that, overall, the percentage of genes that were

395   activated in response to low phosphate in the root tip of the WT and were

396   misregulated in *stop1* and *almt1* ranged between 40% to 95% (Figure 5C). The

397   most affected biological process was "cell wall organization" as evidenced by the

398   reduced number of transcripts from the cluster that were activated in response to

399   low Pi in *stop1* and *almt1* (41 WT; 4 *stop1*; 2 *almt1*). Of the 46 differentially

400   expressed genes included in the "response to phosphate starvation" that were

401   regulated in WT root tips, 46% and 40% (21 *stop1*; 18 *almt1*) were differentially

402   expressed in the root tips of *stop1* and *almt1*, respectively.

403

404   We found that the expression of *SPX1* and *SPX2*, two key genes in the

405   regulation of Pi-responsive genes that are systemically induced (34), were normally

15

406   induced in the root tips of *stop1* and *almt1* mutants (Supplementary File 1).

407   Therefore, we examined the transcription levels of genes that are known targets of

408   the PHR1/SPX systemic regulatory node (6). Of the 94 PHR1 direct targets that we

409   found induced in the root tips of WT plants, we found that 60% (63 *stop1*; 57 *almt1*)

410   were also induced in *stop1* and *almt1* in response to low Pi conditions (Figure 5D).

411   Since the activation of genes in the "cell wall organization" cluster is one of the

412   most affected in *stop1* and *almt1* and its transcriptional regulation has been

413   recently linked to the local response to low Pi availability (35), our results suggest

414   that the local response to low Pi is largely lost in *stop1* and *almt1* and that the

415   systemic response to low Pi is significantly less affected than the local response in

416   these two mutants. To confirm that this was indeed the case, we performed a

417   comparison of genes that had been previously defined to participate in local and

418   systemic responses to low Pi (5) with those that were not activated in *stop1* and

419   *almt1* (Figure 5D). We found that among the 79 systemic and 147 local genes that

420   were differentially expressed in the WT in response to Pi deficiency under our

421   experimental conditions, over 60% of the systemically regulated genes remained

422   responsive in *stop1* (52) and *almt1* (51), while less than 28 % of locally regulated

423   genes (40 *stop1*; 24 *almt1*) remained responsive to Pi starvation in the root tips of

424   the mutants (Figure 5D). These results confirm that *STOP1* and *ALMT1* have a key

425   role in regulating the expression of genes in the local response to Pi deficiency.

426   Nonetheless, *STOP1* and *ALMT1* also seem to have a significant effect on a group

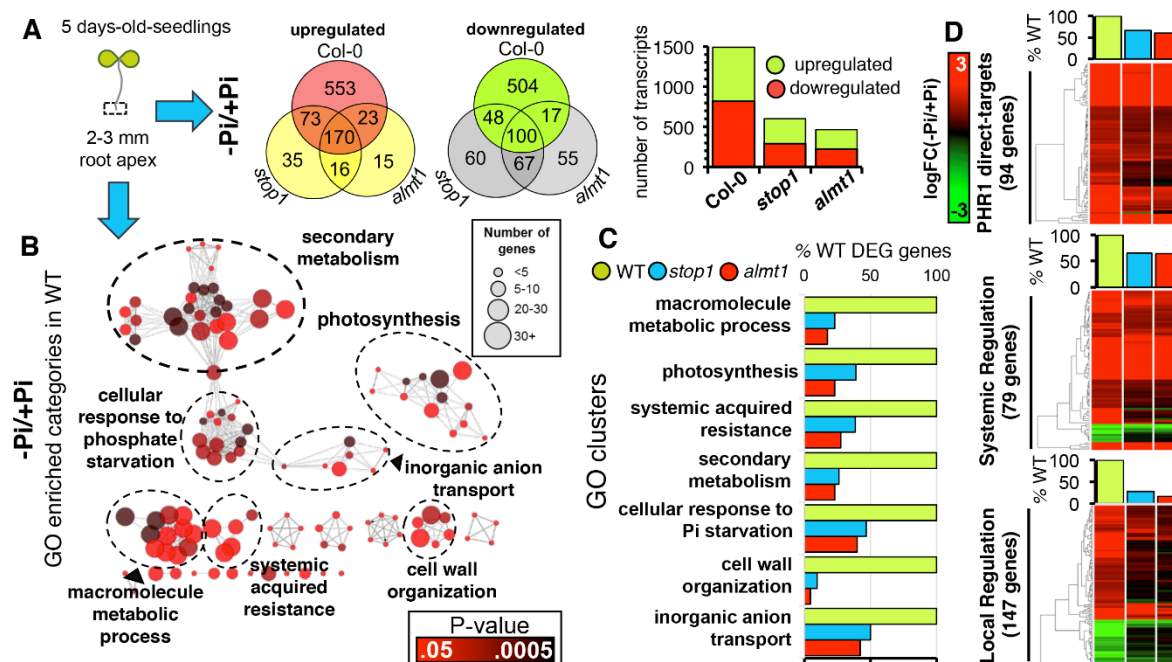427   of genes that are systemically induced by low Pi availability.

428

Figure 5. **Differential expression profiling of WT, *stop1* and *almt1* revealed a loss of transcriptional response to Pi starvation in the root apex of *stop1* and *almt1*.** (A) Venn diagram of differentially expressed genes (DEG) that are up- and down-regulated (-1.5 > logFC(-Pi/Pi) > 1.5; FDR < .05) in the root tip of WT, *stop1* and *almt1* seedlings in response to -Pi conditions. A bar-graph illustrating the number of upregulated and downregulated transcripts in WT, *stop1* and *almt1* is presented. (B) Gene Ontology (GO) enrichment analysis of overrepresented categories that are activated in the root apex of Pi-deprived WT seedlings. Each circle corresponds to a significantly enriched GO category (P-value <.05; hypergeometric test; Benjamini-Hochberg correction). Color code resembles P-value and size resembles the number of genes that are associated to that respective GO category. GO categories that share genes are connected and clustered by the biological process that corresponds to the most significantly enriched category of the cluster. (C) Analysis of DEG by cluster in the root tip of *stop1* and *almt1*. The number of genes that belong to each GO cluster and are differentially expressed in *stop1* and *almt1* is presented as a percentage of the number of genes that are differentially expressed in WT (% DEG of WT). (D) Transcriptomic analysis of locally and systemically regulated genes in the root apex of WT, *stop1* and *almt1* revealed a key role of *STOP1* and *ALMT1* in the local response to Pi starvation in *Arabidopsis*. WT, *stop1* and *almt1* logFC values of genes that are differentially expressed in the root tips of WT seedlings (-1.5 > logFC(-Pi/Pi) > 1.5; FDR < .05) in response to -Pi conditions and were reported as PHR1-direct targets (6) and of those that were classified as part of the local or systemic transcriptional response as reported by (5) is represented in a heatmap, respectively. Genes that are differentially expressed in WT root tips and their expression levels in WT, *stop1* and *almt1* seedlings grown under -Pi conditions are illustrated according to the key.

453 **Malate treatment rescued the expression of local-response genes**
454 **encoding apoplast-located proteins**

455

456 As we observed that malate treatment rescued iron accumulation in the
457 RAM and the long root phenotype of *stop1* and *almt1* mutants, we sought to
458 identify the subset of genes that regulate primary root growth inhibition and whose
459 expression under low Pi conditions is re-activated by malate treatment in *stop1* and
460 *almt1* seedlings. To this end, we isolated mRNA from the root tips of Pi-deprived
461 *stop1* and *almt1* mutants that were treated with malate (1 mM) and carried out
462 RNA-seq analysis (Figure 6). Our rationale was that the common set of genes that
463 are differentially expressed in the root tips of Pi-deprived seedlings that have a
464 short-root phenotype (WT, *stop1*+M, *almt1*+M) and that are not differentially
465 expressed (induced or repressed) in the root tips of Pi-deprived *stop1* and *almt1*
466 seedlings, which have a long root phenotype in -Pi media, are linked to the malate-
467 dependent mechanism that triggers primary root growth inhibition under Pi
468 deprivation conditions. A common set of 210 differentially expressed genes (63
469 upregulated; 147 downregulated) was found between the genotypes/treatment that
470 induce a short root phenotype under -Pi conditions and that are not differentially
471 expressed in Pi-deprived seedlings with a long root phenotype (Figure 6A). Among
472 the genes whose expression was rescued by malate treatment, we found several
473 peroxidase family genes (*PEROXIDASE2, PEROXIDASE37, AT3G01190,*
474 *PEROXIDASE4*) which are closely related to the control of ROS homeostasis (36).
475 A full list of the genes and description is included in Supplementary File 1.
476 Interestingly, using SUBA, a subcellular prediction tool (Tanz et al. 2013), we found
477 that 30% of proteins encoded by genes whose responsiveness to low Pi is restored
478 by malate treatment in *stop1* and *almt1* Pi-deprived seedlings are targeted to the
479 apoplast or extracellular region (Figure 6B), confirming a previous study in which a
480 major role of the apoplast in the root response to Pi starvation was highlighted (35).
481 Furthermore, an additional 16% of genes are targeted to the plasma membrane
482 (Figure 6B).

483

484

485

486 **Figure 6. Malate treatment rescues the expression of transcripts whose products are**
487 **targeted to the extracellular region.** (A) Schematic of the Venn diagram analysis of
488 common differentially expressed genes (DEG; -1.5 > logFC(-Pi/Pi) > 1.5; FDR < .05) in
489 short-root phenotypes (WT∩*stop1*∩*almt1*) minus the DEG in long-root phenotypes
490 (*stop1*∪*almt1*) under Pi deficiency conditions, that was performed to determine the genes
491 whose expression is linked to short-root phenotype and is rescued by malate treatment in
492 *stop1* and *almt1* seedlings. A heatmap of the logFC values in WT, *stop1/*+M and *almt1/*+M
493 of the determined gene set is presented. (B) Predicted subcellular location of the DEG
494 whose expression is restored by malate treatment. (C) *LPR1*, *UPBEAT1* and *VTC4*
495 expression levels are presented in fold change (FC; FDR<.05) as revealed by our
496 transcriptomic studies in the root apex of WT, *stop1* and *almt1* seedlings under -Pi
497 conditions and -Pi and malate treatment (*almt1*+M, *stop1*+M) conditions.

498

499

19

500

LPR1 acts downstream of STOP1 and ALMT1

502

In *Arabidopsis*, *LPR1* has been reported to mediate the oxidation of Fe^{2+} to Fe^{3+} in the apoplast, which was correlated with ROS generation that triggers callose deposition in the root apex and disrupts SHR transport which ultimately induces determinate primary root growth in response to Pi deficiency conditions [20]. As both Fe^{3+} accumulation and the regulation of peroxidases are lost and rescued by malate treatment in *stop1* and *almt1* mutants, using our RNASeq data, we analyzed if malate treatment had the same effect on the *LPR1* expression in response to low Pi conditions in the root apex of *stop1* and *almt1* (Figure 6C). The expression of *LPR1* was found to be enhanced in the root apex of WT seedlings (3.29 fold) exposed to low-Pi, induction that was significantly lower in *stop1* (1.64 fold) and *almt1* (1.25 fold) Pi-deprived seedlings (Figure 6C). Our data revealed that, indeed, malate treatment increased *LPR1* transcript levels in Pi-deprived *stop1* seedlings from 1.5 to 2.0-fold and in *almt1* seedlings from 1.2 to 2.7-fold (Figure 6C). The higher increase in *LPR1* expression induced by malate treatment in *almt1* than *stop1* correlates with the capacity of the treatment to better restore the primary root response to low in *almt1* than *stop1* (Figure 6C). To test whether the effect of malate was dependent or independent of LPR1, we studied the effect of malate treatment on the primary root elongation of *lpr1* seedlings grown in media lacking Pi. We observed that malate treatment did not rescue the *lpr1* mutant phenotype (Supplementary Figure 6), suggesting that the effect of malate to trigger the determinate root developmental program in response to Pi deficiency requires the presence of a functional LPR1 protein.

525

Since alterations in the ROS balance in the RAM of *Arabidopsis* are linked to the meristem exhaustion process observed in Pi-deprived seedlings [37] and *LPR1* is essential for the low-Pi dependent ROS signaling that takes place in the primary root of *Arabidopsis*, we decided to analyze the transcript levels of *UPBEAT1* (*UPB1;* Figure 6C*)*; the only transcription factor known to module ROS

531 balance and control the transition from cell proliferation to cell differentiation in the

532 RAM by modulating the transcription of peroxidase genes (38). We observed that

533 *UPBEAT1* is down-regulated 0.48-fold in response to low Pi in the root apex of WT

534 seedlings and that it is downregulated to a lower degree in *stop1* (0.64 FC) and

535 *almt1* (0.67 FC). Malate treatment restored the downregulation of *UPB1* in Pi-

536 deprived *almt1* (0.46 FC) and *stop1* (0.37 FC) seedlings to WT levels (Figure 6C).

537 Since LPR1 and UPB1 seem to be involved in modulating ROS balance in the

538 RAM and their expression is misregulated in *stop1* and *almt1*, we identified

539 peroxidase genes which have been related with ROS homeostasis in the root (36)

540 and analyzed their expression levels in WT, *stop1* and *almt1* seedlings. We found

541 that 18 peroxidase genes *(PRXS)* were transcriptionally regulated by low Pi in the

542 root apex of WT seedlings of which 13 *PRXS* were not responsive to low Pi in

543 *stop1* and *almt1* (Supplementary File 1). Interestingly, the responsiveness of 11

544 peroxidase genes *(PEROXIDASE52, AT4G08780, AT4G08780, PEROXIDASE2,*

545 *AT5G06730, AT5G39580, PEROXIDASE37, AT5G15180, PEROXIDASE4,*

546 *AT2G39040, AT3G01190)* was rescued by malate treatment in Pi-deprived *stop1*

547 and *almt1* seedlings (Supplementary Figure 7). Alterations of ROS balance have

548 been related to callose deposition in the primary root of *Arabidopsis* (20). Given

549 that the transcription of ROS-related genes *(UPB1, LPR1 and PRXS)* is disrupted

550 in *stop1* and *almt1* under low Pi conditions, we analyzed the expression values of

551 genes coding for callose synthases *(CALS)*. We found that the expression of 4

552 genes coding for *CALS (CALLOSESYNTHASE7, CALLOSESYNTHASE9,*

553 *GLUCANSYNTHASELIKE4, GLUCANSYNTHASELIKE5)* was induced (1.1 logFC;

554 FDR<.05) in the root apex of WT seedlings and that it was induced to a lesser

555 extent (logFC<0.6) in *stop1* and *almt1* seedlings. It was observed that malate

556 treatment also rescued the expression of these 4 *CALS* in Pi-deprived *stop1* and

557 *almt1* (Supplementary Figure 7). Our results suggested that malate efflux is

558 required for the ROS signaling cascade that has been reported to be affected in

559 low-Pi insensitive mutants (20, 37).

560

561 Given that Fe tends to its higher oxidation state (Fe^{3+}) in natural

562 environments and the iron uptake genes *IRON REGULATED TRANSPORTER 1*

563 (*IRT1*) and *FERRIC REDUCTION OXIDASE 2* (*FRO2*) have been reported to be

564 repressed in response to Pi deficiency conditions (3, 5, 39) we asked whether an

565 alternative Fe^{3+} reduction mechanism could provide Fe^{2+} to LPR1 to initiate the

566 proposed ROS signaling cascade that is induced in the RAM in response to low Pi.

567 An ascorbate dependent Fe^{2+} reduction mechanism has been reported recently

568 (31), in which *VITAMINC4* (*VTC4*), a gene encoding a protein with dual myo-

569 inositol-monophosphatase and ascorbate synthase activity (40), could play a

570 central role. We found that *VTC4* is induced in the root apex of WT (5 FC), *almt1*

571 (4.3 FC) and *stop1* (3.22 FC) seedlings (Figure 6C). Interestingly, *VTC4* belongs to

572 the set of genes that are direct targets of PHR1 (6), providing a potential link

573 between local and systemic signaling in the primary root response to low Pi and

574 the crosstalk between Fe and P in the Pi deficiency response.

575

576 **Discussion**

577

578 LPR1 has been proposed to promote the accumulation of Fe in the apoplast

579 of cells in the RAM, which in turn triggers an accumulation of callose that alters

580 symplastic transport causing meristem differentiation (20). However, the precise

581 mechanism by which Fe accumulates in the apoplast of RAM cells remained to be

582 determined. Here we show that *STOP1* and *ALMT1* participate in the mechanism

583 that triggers RAM exhaustion in response low Pi availability by mediating the

584 accumulation of Fe^{3+} in the apoplast of RAM cells. *STOP1* and *ALMT1* were

585 originally described as genes responsible of the malate efflux that protects the

586 *Arabidopsis* root from Al^{3+} toxicity (21, 22). *AtSTOP1* is constitutively expressed in

587 *Arabidopsis*, indicating that its involvement in the Al-dependent induction of gene

588 expression must involve posttranslational processes of modification or the direct

589 binding of Al^{+3}. The finding that mutations in *STOP1* and *ALMT1* lead to long root

590 phenotypes in Pi-deprived seedlings suggests that malate excretion is also

591   involved in the process of meristem exhaustion in response to low Pi availability.
592   We found that *STOP1* is expressed in the RAM in a Pi-independent fashion and
593   that *ALMT1* is expressed in the RAM but only in seedlings grown in media with low
594   Pi concentrations. Although the expression domains of *STOP1* and *ALMT1* do not
595   completely overlap, we found that the expression directed by the *ALMT1* promoter
596   is completely dependent on an intact copy of *STOP1* (Supplementary Figure 2).
597   The apparent inconsistency between the role of an activator with its target gene
598   and the differences in patterns of expression of *STOP1* and *ALMT1* could be
599   explained by the recent report that *STOP1* mRNA is cell-to-cell mobile (42).

600

601   Pi and Fe availability have been shown to coordinately regulate RAM
602   maintenance and primary root growth in vitro (11, 17, 20). Our results corroborate
603   that, in *Arabidopsis* WT seedlings, Fe availability (Supplementary Figure 8) in the
604   medium is required for RAM-exhaustion in media with a low Pi concentration and
605   that Fe accumulation in the RAM is associated with the process of RAM-
606   exhaustion (Figure 4). Apoplastic iron accumulation in the RAM was reported to be
607   essential for primary root growth inhibition in response to -Pi conditions (20),
608   however, the mechanism for iron accumulation in the root remained to be
609   determined. We found that Fe failed to accumulate in the root apex of *stop1* and
610   *almt1* seedlings grown in Pi-deficient media and that the treatment of *stop1* and
611   *almt1* seedlings with malate restores both Fe accumulation in the RAM and the
612   inhibition of primary root growth in Pi-deprived seedlings (Figure 4). These data
613   show that malate secretion is necessary and sufficient for iron accumulation in the
614   RAM and to trigger cell differentiation in the RAM that is responsible for the
615   meristem exhaustion process induced by Pi deficiency. We propose that such
616   mechanism of iron accumulation happens in the apoplast as ALMT1 is reported to
617   be a malate efflux protein (22) and thus, exogenous malate, which probably
618   diffuses through the apoplast, can rescue iron accumulation in *almt1* and *stop1*.
619   Malate supplementation was found to fully rescue the short-root phenotype of
620   *almt1* while it only partially restored primary root growth inhibition in *stop1*,

23

621 suggesting that, in addition to *ALMT1*, *STOP1* regulates the expression of other
622 genes whose activation by low Pi is required for full meristem exhaustion.

623

624   Molecular dynamic simulation of Fe^{3+} and Fe^{2+} interaction shows that malate
625 can form large complexes with Fe^{+3} but not Fe^{+2} (Supplementary Figure 5). This
626 data suggests that malate promotes the accumulation of Fe^{+3} in the apoplast by
627 forming these large molecular weight complexes, which by a still largely unknown
628 mechanism that correlates with ROS generation [20], activate the processes
629 required for meristem exhaustion. *lpr1* seedlings also show a long root phenotype
630 in low Pi media, suggesting that the ferroxidase activity of LPR1 is required to
631 trigger cell differentiation during the primary root meristem exhaustion process
632 triggered by Pi-deprivation. We found that the long root phenotype of *lpr1* in low-Pi
633 media cannot be rescued by malate treatment, suggesting that *LPR1* acts
634 downstream of *STOP1* and *ALMT1* and that most probably is required to activate
635 the Fe-mediated mechanism involved in the process of RAM exhaustion observed
636 in Pi-deprived seedlings. Therefore, cell-wall-localized LPR1 ferroxidase activity
637 which catalyzes Fe^{+2} to Fe^{+3} conversion [20], could act synergistically with malate
638 efflux in the accumulation of Fe^{3+} in the apoplast of RAM cells. LPR1-dependent
639 Fe^{3+} production in the apoplast could trigger ROS production by initiating a Fe
640 redox cycle as previously proposed [43]. Either ferric-chelate reductase oxidase
641 activity, which reduces apoplast-diffusible Fe^{3+} chelates, or effluxed ascorbate [31]
642 could reduce the Fe^{3+} produced by LPR1 to a redox-active Fe^{2+} to complete a
643 cycle thereby triggering root cell differentiation. Supporting this notion, *LPR1*
644 overexpression causes ectopic Fe^{3+} and ROS generation in Pi-deprived seedlings
645 [20]. Our data suggest the existence of a *STOP1, ALMT1* and *LPR1* coordinated
646 redox mechanism that involves Fe^{+3} deposition in the apoplast of RAM cells of
647 seedlings exposed to low Pi. *ALMT1* is transcriptionally upregulated in a similar
648 fashion in WT and *lpr1* mutants [35], confirming that LPR1 acts downstream of the
649 STOP1/*ALMT1* low Pi regulatory node.

650

651   Expression of up to 80% of the genes involved in the local response to low
652   Pi was affected in *stop1* and *almt1*, whereas less than 40% of Pi systemically
653   responsive genes were affected in the same mutants (Figure 5D). These results
654   show that, in addition to controlling the primary root developmental response to low
655   Pi, *STOP1* and *ALMT1* play an important role in modulating the transcription of
656   other genes involved in the local response to Pi starvation. However, the reduction
657   in both local and systemic responses in *stop1* and *almt1* points to a cross-talk
658   between the signaling pathways that regulates the transcriptional activation or
659   repression of the systemic and local responses to low Pi in the root apex. However,
660   we cannot rule out the possibility that the internal concentration of Pi could be
661   higher in the root tip of *stop1* and *almt1* than the WT, which could lead to a
662   downregulation of the systemic response, as has been observed in plants grown in
663   low Pi and low Fe conditions (17). Further experiments regarding a possible
664   STOP1 and ALMT1 interaction directly with Pi, PHR1 or SPX-domain proteins
665   could shed light on the existence of a coordinated response to external and internal
666   Pi levels in the root apex. The observation that PHR1 activates the expression of
667   the ascorbate synthase *VTC*4 under Pi deficiency conditions together with the
668   recent report that ascorbate efflux contributes to Fe^{3+} reduction (31), support the
669   notion that the redox cycle that generates ROS and triggers RAM exhaustion could
670   be controlled by both local and systemic responses to Pi starvation.

671

672   Our transcriptomic analysis revealed that *LPR1* is responsive to Pi-
673   deprivation in the root tips of WT plants (Figure 6C) and that this response is
674   significantly reduced in the root tips of *stop1* and *almt1* seedlings (Figure 6C).
675   These results suggest that a threshold level of *LPR1* is required to activate
676   meristem exhaustion in Pi-deprived seedlings. This notion is supported by the
677   observation that the treatment with malate that reverts the long root phenotype of
678   Pi-deprived *stop1* and *almt1* seedlings (Figure 4A) also leads to an increase in
679   *LPR1* transcript levels (Figure 6C). Moreover, *Arabidopsis* accessions with higher
680   *LPR1* transcription levels have shorter primary roots under low Pi conditions (16)
681   and we observed that, in the case of malate-treated Pi-deprived *stop1* and *almt1*

25

682   seedlings, a higher *LPR1* expression in *almt1* than in *stop1* correlated with a
683   shorter primary root in *almt1* than *stop1* (Figure 4B, 6C). A recent report on the
684   interplay between the transcriptional activation of genes coding for extracellular
685   enzymes and iron-redistribution in the apoplast in response to Pi-deprivation
686   highlighted the role of the apoplast in the Pi starvation response (35).
687   Transcriptomic analysis of Pi-deprived *stop1* and *almt1* seedlings showed that
688   malate treatment reactivates the low-Pi-responsiveness of genes that encode
689   extracellular proteins involved in cell-wall modification and ROS homeostasis, such
690   as peroxidases (36). Our transcriptomic results confirm a previously reported role
691   of apoplastic peroxidases in the Pi starvation response (35), and highlight the role
692   of malate secretion in the cell wall remodeling processes potentially involved in the
693   changes of *Arabidopsis* root system architecture induced by low Pi availability. In
694   this context, the finding that *UPBEAT1,* a transcription factor that modulates the
695   transition from cell proliferation to cell differentiation in the RAM by repressing
696   peroxidase genes (38), is repressed in response to Pi deficiency conditions and the
697   fact its expression is altered in *stop1* and *almt1*, support the notion that ROS
698   generation plays an important role in the root response to Pi deprivation. Further
699   experiments regarding the specific pattern of ROS signaling in the RAM under Pi
700   starvation conditions are required.

701

702   A model that summarizes what is known about the local response to Pi
703   starvation and the proposed role of *STOP1* and *ALMT1* in the root response to Pi
704   deprivation is presented in Figure 7. Under Pi deficiency conditions, expression of
705   LPR1 is enhanced by a malate-dependent mechanism and PDR2 activity is
706   inhibited facilitating LPR1 mobilization from the ER to the plasma membrane (20)
707   where LPR1 ferroxidase activity catalyzes Fe^{2+} to Fe^{3+} conversion in the apoplast of
708   RAM cells (Figure 7). The mechanisms by which LPR1 is transported from the ER
709   to the extracellular region and how PDR2 activity is regulated by Pi-availability
710   remain to be determined. *STOP1, a* constitutively expressed gene, up-regulates
711   the expression of *ALMT1* in seedlings exposed to low Pi, thereby activating the
712   excretion of malate. LPR1 ferroxidase activity in the plasma membrane of cells in

713   the meristem and elongation zones of the primary root locally produces Fe^{3+} which
714   forms large complexes with malate, leading to its accumulation. Expression of the
715   ascorbate synthase *VTC*4 under Pi deficiency conditions is activated and the
716   presence of ascorbate in the apoplast produces the Fe^{2+} required to complete a
717   redox cycle that generates ROS. Expression of the *UPB1* repressor is reduced by
718   a Fe/malate-dependent mechanism under low Pi conditions, which enhances the
719   transcription of peroxidase genes. Enhanced transcription of local response
720   peroxidase genes likely triggers ROS generation in the root of Pi-deprived
721   seedlings as previously reported [37]. ROS generation triggers callose deposition
722   as previously reported [20, 44]. This notion is supported by the observation that the
723   expression of several *CALS* genes is enhanced in the root apex of WT but not in
724   *stop1* and *almt1* seedlings (Supplementary Figure 7). Callose synthesis impairs
725   symplastic transport by physically blocking plasmodematal pores, which reduces or
726   inactivates the cell to cell movement of SHR [20]. Since SHR cell to cell movement
727   is required for stem cell niche maintenance, meristem exhaustion takes place in
728   seedlings exposed to low Pi availability. However, since CLE-like peptide signaling
729   is also required for stem cell niche maintenance in *Arabidopsis* [45] we cannot rule
730   out that ROS or Fe^{3+} accumulation in the RAM could induce the transcription of
731   CLE peptides that could also execute RAM exhaustion.

732

733   STOP1 controls *ALMT1* transcription and its expression is not regulated by
734   Pi availability, suggesting that STOP1 is most likely involved in sensing external Pi-
735   levels or an environmental cue that it is linked to low-Pi levels in the medium. Since
736   STOP1 also controls low pH and Al^{3+} toxicity responses, it emerges as a possible
737   master regulator/sensor that orchestrates the root responses to multiple
738   environmental stresses.
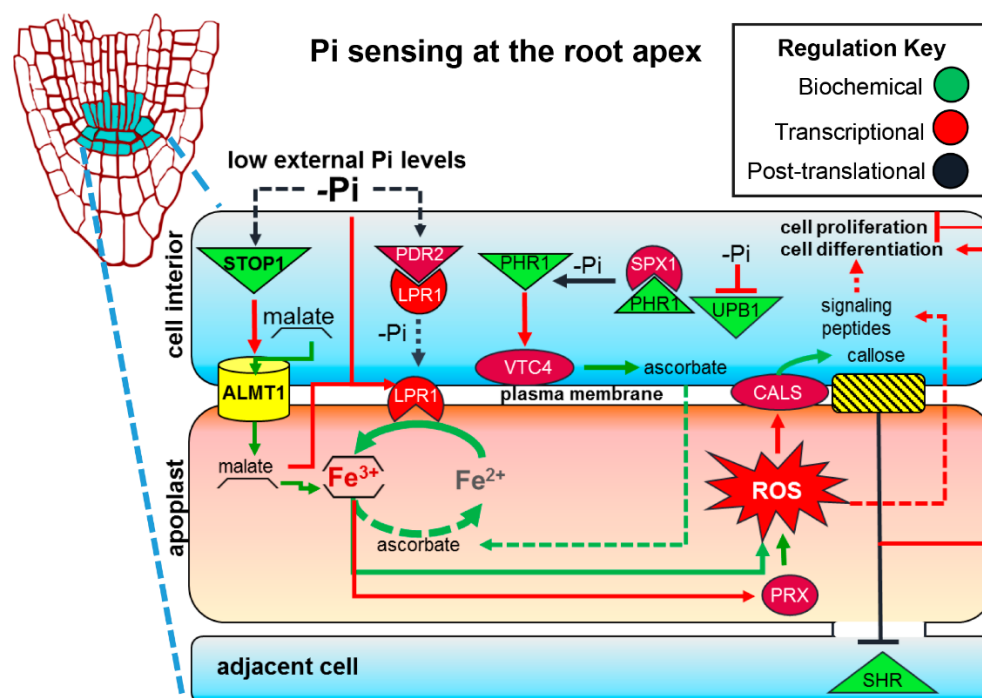
Figure 7. *STOP1* and *ALMT1* regulate the RAM response to low Pi conditions in *Arabidopsis.* In response to limiting Pi levels in the medium, *STOP1* induces *ALMT1* (Figure 3) which triggers malate efflux in the root apex. Low Pi levels also inhibit PDR2 negative regulation over LPR1 and induce, in a largely unknown mechanism, LPR1 transport to the plasma membrane. Malate contributes to the aggregation of Fe^{3+} ions in the apoplast and enhances the expression of *LPR1*, callose synthase genes (*CALS*) peroxidase genes (*PRX*) under Pi deficiency conditions. LPR1 and PRX activity generates reactive oxygen species (ROS) which enhance callose deposition by CALS. Callose deposition closes the symplastic channels of communication which ultimately impairs the transport of transcription factors, such as SHR, that are essential to maintain cell proliferation and organization in the RAM. Alternative factors induced by ROS, such as signaling peptides, could also induce cell differentiation in the RAM. A crosstalk between internal sensing, mediated by the PHR1/SPX1 module, and external Pi-sensing could be interconnected by ascorbate efflux into the apoplast, which can reduce Fe^{3+} to Fe^{2+} and could re-start the proposed redox cycle. Ascorbate can be produced by VTC4 whose gene is induced by PHR1 when internal Pi levels are limiting. Arrows represent relationships between the components. Dotted lines represent hypothetical relations, and the regulation key illustrates the type of evidence that has been provided for that relationship.

Materials and Methods

28

Plant material

Arabidopsis thaliana Col-0 accesion (CS70000) was used in this work. Stop1-SALK_114108 (N614108), almt1-SALK_009629 (N509629), and lpr1 (N516297) lines were provided by the NASC (European Arabidopsis Stock Center).

Growing conditions

Seeds were surface sterilized and sowed in 1% agar, 0.1x MS medium as described by (10). 1mM KH_2PO_4 (high Pi; +Pi) or 10µM KH_2PO_4 (low Pi; -Pi) Pi concentrations were used. 1% (w/v) sucrose and 3.5mM MES was added. Fe-free medium was prepared as described (15), and 100µM ferrozine (SIGMA-82950) was added to reduce agar Fe-availability. Malate and citrate (SIGMA-M1000 and SIGMA-C0759, respectively) were added to medium before sterilization. Seedlings were grown in a Percival chamber at 22 ºC, under 16/8 hrs photoperiod with >200 µmol*m-2*-1 luminous intensity.

EMS mutagenesis

Over 3000 *Arabidopsis* seeds were surface sterilized with ethanol 95% (v/v) ethanol for 10min and 20% (v/v) bleach for 6 min. The sterilized seeds were left overnight at 4°C on a rocker in distilled water. Then seeds were incubated with 0.04% EMS (SIGMA-M0880) during in 100 mM sodium phosphate buffer, pH7. After 9 hours the seeds were washed ten times with distilled water to remove EMS residues. EMS mutagenized seeds (M1) were propagated under greenhouse conditions and F1 seeds (M2) were harvested and grown under -Pi conditions. Mutants that presented a long-root phenotype under in -Pi media were selected.

Gene mapping

Plant mapping populations were built crossing *lpi5* and *lpi6* homozygous lines vs Col-0 (CS70000) respectively, according to the Mutmap protocol (26). Heterozygous F1 plants were self-fertilized for seed propagation. The F2 segregating individuals, were re-screened for WT (short root) and mutant (long

791 root) phenotypes, respectively for each of the two crosses. Then, DNA was
792 extracted from 100 plants for each phenotype, pooled and sequenced using
793 Illumina Miseq technology (paired-end, 250 base-pair reads length and 50X
794 coverage). Reads obtained were processed with fastQC and Trimmomatic (46) to
795 improve their quality. Only paired-end reads were considered. Reads were mapped
796 to the Col-0 reference genome (TAIR10) using BWA (47) and SAMtools (48). To
797 identify and to evaluate specific variants related with the mutant phenotype (long
798 root) a pipeline using GATK (https://software.broadinstitute.org/gatk/), VCFtools
799 (49), SNPeff and SNPshif (27) was implemented. IGV was used to visualize the
800 variants analyzed (50).

801

802   Transcriptional reporter lines
803   Transgenic Col-0 plants harboring transcriptional gene fusions containing
804 the *STOP1* and *ALMT1* promoter regions, respectively, fused to a double GFP-
805 G U S r e p o r t e r g e n e w e r e p r o d u c e d u s i n g 4900pb (primers:
806 s t o p 1 F w : G A A C G A C A A G A T T A C A A G T A G G T T C   a n d
807 stop1Rv:GTTGCACAAATCGTCTTCAGTTTCC) and 2253 (primers:
808 a l m t 1 F w : G G C A G A T A A A G A G G C A C T C G T G   a n d
809 almt1Rv:CTCTCTCACTTTCTCCATAACACC) intergenic regions of *STOP1* and
810 *ALMT1*, respectively, were used to build the *proSTOP1::GUS-GFP* and
811 *proALMT1::GUS-GFP* transcriptional reporter lines respectively. Intergenic region
812 were cloned on the pKGWFS7 using the Gateway system. *Arabidopsis* plants were
813 agro-infiltrated using the floral-dip method (51).

814

815   Histochemical GUS staining
816 Histochemical GUS staining was performed as reported by (52). The stained roots
817 were clarified following the protocol reported by (53). A representative root stained
818 was chosen and photographed using Nomarski optics on a Leica DMR
819 microscope.

820

821

30

822

823   Histochemical iron staining

824 Perls iron staining and DAB intensification were carried out as described in [20]

825 and analyzed using Nomarski optics on a Leica DMR microscope.

826

827   Malate and Fe(II), Fe(III) and Al(III) Molecular Dynamics

828 Molecular dynamic (MD) calculations were carried out to obtain insight about the

829 behavior between malate molecules and Fe(II), Fe(III) and Al(III) ions in explicit

830 water solution. Non-bonded parameters for the metallic cations were taken from

831 the 12-6-4 Lennard-Jones-type non-bonded model for divalent [54] and highly

832 charged metal ions [55] respectively. These parameters were then adapted to the

833 GROMOS 53a6 force field and integrated with GROMACS 5.0 as a user specified

834 non-bonded potential employing tabulated interaction functions [56]. The all-atom

835 PDB optimized geometry structure and parameters for malate molecules were

836 taken from the ATB web server [57]. A total of nine systems were built with the

837 malate-Fe(II), malate-Fe(III) and malate-Al(III) proportions of 0:120, 40:120, 80:120

838 and 120:120 within a cubic box with periodic boundary conditions. In all systems,

839 the box was solvated with SPC/E [58] type water molecules and the steepest

840 descents method was employed to minimize the energy. The temperature was set

841 to 300 K and an equilibration phase of 100 ps in the canonical ensemble (NVT)

842 was conducted using the V-rescale algorithm [59]. Long-range electrostatics were

843 calculated employing the PME method [60, 61] with a cutoff of 12 Å and the same

844 cutoff was chosen for the van der Walls non-bonded interactions. All bond lengths

845 were constrained with Linear Constraint Solver (LINCS; [62]. A final production of

846 50 ns in the isothermal-isobaric ensemble (NPT) was conducted using the

847 Parrinello-Rahman algorithm [63]. Snapshots were stored after each 10 ps and the

848 final MD trajectories were analyzed using the g_aggregate tool [64].

849

850   Preparation of root tip mRNA-seq libraries

851 Total RNA was isolated from frozen root tip powder using TRIzol reagent

852 (Invitrogen) according to the manufacturer's instructions. Frozen root tip powder

853 was obtained from root tip sections of approximately 2-3 mm length from
854 approximately 500 individuals per treatment (5 dag). Non-strand specific mRNA-
855 seq libraries were generated from 5 µg of total RNA and prepared using the TruSeq
856 RNA Sample Prep kit (Illumina) according to the manufacturer's instructions.

857

858 RNA-seq High-throughput Sequencing and Data Analysis
859 High-throughput sequencing and data analysis were carried out as in (65). Briefly,
860 quality assessment of the reads generated with the Illumina analysis pipeline (fastq
861 format) was performed using FastQC (version 0.11.4) and processed using
862 Trimmomatic (46) (version 0.35) to remove reads that contained adapter
863 sequences and low quality reads. Single and paired-end clean reads were aligned
864 to the Arabidopsis thaliana TAIR10 reference sequence using TopHat2 (66)
865 (version 2.0.9). Raw counts per gene were estimated using HTseq (67) (version
866 0.6.0). Data was normalized in edgeR (68) (version 3.12.0) using the trimmed
867 mean of M values (TMM) method. Genes with ≥ 3 reads in total, across all
868 samples, were included in the final analysis. Transcript abundance as represented
869 by the normalized raw counts per gene was used to determine differential
870 expression using the edgeR package. Analysis of GO enriched categories and
871 clusterization into functional groups by biological process was performed using
872 Cytoscape (69) (version 3.4) plugin ClueGO+CluePedia (70).

873

874 qRT-PCR
875 Total RNA was isolated using TRIzol reagent (Invitrogen) according to the
876 manufacturer's instructions. Real-time PCR was performed with an Applied
877 Biosystems 7500 real-time PCR system using SYBR Green detection chemistry
878 (Applied Biosystems) and gene-specific primers. The relative expression levels
879 were computed by the Ct method of relative quantification. Oligonucleotide primer
880 sequences are available upon request.

881

882 **Acknowledgements**

Competing Interest

The authors declare no competing interest.

Supplementary File 1 (.xlsx format) is deposited in the following link:

https://www.dropbox.com/s/u5fv1wbrcmd1th6/Supplementary%20File%201.xlsx?dl=0

Genomic data generated in this study is accessible at www.ncbi.nlm.nih.gov/biosample/
Accession codes:
WT-*lpi5*: SAMN06013467; Mutant-*lpi5*: SAMN06013468; WT-*lpi6*: SAMN06013469;
Mutant-*lpi6*: SAMN06013470;
http://www.ncbi.nlm.nih.gov/biosample/6013467
http://www.ncbi.nlm.nih.gov/biosample/6013468
http://www.ncbi.nlm.nih.gov/biosample/6013469
http://www.ncbi.nlm.nih.gov/biosample/6013470

Expression data generated in this study is deposited in the Gene Expression Omnibus database (GSE90061) and can be accessed at:

https://www.ncbi.nlm.nih.gov/geo/query/acc.cgi?token=gfybucyuzbwrdyn&acc=GSE90061

References

1. Marschner H (2011) *Marschner's Mineral Nutrition of Higher Plants* (Elsevier Science) Available at: https://books.google.com.mx/books?id=yqKV3USG41cC.

2. Wu P, et al. (2003) Phosphate starvation triggers distinct alterations of genome expression in Arabidopsis roots and leaves. *Plant Physiol* 132(3):1260–1271.

3. Misson J, et al. (2005) A genome-wide transcriptional analysis using Arabidopsis thaliana Affymetrix gene chips determined plant responses to phosphate deprivation. *Proc Natl Acad Sci U S A* 102(33):11934–11939.

919   4. Morcuende R, et al. (2007) Genome-wide reprogramming of metabolism and
920   regulatory networks of Arabidopsis in response to phosphorus. *Plant Cell Environ*
921   30(1):85–112.

922   5. Thibaud MC, et al. (2010) Dissection of local and systemic transcriptional responses
923   to phosphate starvation in Arabidopsis. *Plant J* 64(5):775–789.

924   6. Bustos R, et al. (2010) A Central Regulatory System Largely Controls Transcriptional
925   Activation and Repression Responses to Phosphate Starvation in Arabidopsis. *PLoS*
926   *Genet* 6(9):e1001102.

927   7. Hoffland E, Van Den Boogaard R, Nelemans J, Findenegg G (1992) Biosynthesis and
928   root exudation of citric and malic acids in phosphate-starved rape plants. *New Phytol*
929   122(4):675–680.

930   8. Cruz-Ramirez A, Oropeza-Aburto A, Razo-Hernandez F, Ramirez-Chavez E, Herrera-
931   Estrella L (2006) Phospholipase DZ2 plays an important role in extraplastidic
932   galactolipid biosynthesis and phosphate recycling in Arabidopsis roots. *Proceedings*
933   *of the National Academy of Sciences* 103(17):6765–6770.

934   9. Bates TR, Lynch JP (1996) Stimulation of root hair elongation in Arabidopsis thaliana
935   by low phosphorus availability. *Plant Cell Environ* 19(5):529–538.

936 10. Lopez-Bucio J, et al. (2002) Phosphate Availability Alters Architecture and Causes
937   Changes in Hormone Sensitivity in the Arabidopsis Root System. *Plant Physiol*
938   129(1):244–256.

939 11. Sánchez-Calderón L, et al. (2005) Phosphate starvation induces a determinate
940   developmental program in the roots of Arabidopsis thaliana. *Plant Cell Physiol*
941   46(1):174–184.

942 12. Péret B, et al. (2011) Root developmental adaptation to phosphate starvation: better
943   safe than sorry. *Trends Plant Sci* 16(8):442–450.

944 13. Rubio V, et al. (2001) A conserved MYB transcription factor involved in phosphate
945   starvation signaling both in vascular plants and in unicellular algae. *Genes Dev*
946   15(16):2122–2133.

947 14. Raghothama KG (1999) Phosphate Acquisition. *Annu Rev Plant Physiol Plant Mol*
948   *Biol* 50:665–693.

949 15. Sánchez-Calderón L, et al. (2006) Characterization of low phosphorus insensitive
950   mutants reveals a crosstalk between low phosphorus-induced determinate root
951   development and the activation of genes involved in the adaptation of Arabidopsis to
952   phosphorus deficiency. *Plant Physiol* 140(3):879–889.

953 16. Svistoonoff S, et al. (2007) Root tip contact with low-phosphate media reprograms
954   plant root architecture. *Nat Genet* 39(6):792–796.

955 17. Ward JT, Lahner B, Yakubova E, Salt DE, Raghothama KG (2008) The effect of iron
956   on the primary root elongation of Arabidopsis during phosphate deficiency. *Plant*
957   *Physiol* 147(3):1181–1191.

18. Ticconi CA, Delatorre CA, Lahner B, Salt DE, Abel S (2004) Arabidopsis pdr2 reveals a phosphate-sensitive checkpoint in root development. *Plant J* 37(6):801–814.

19. Ticconi CA, et al. (2009) ER-resident proteins PDR2 and LPR1 mediate the developmental response of root meristems to phosphate availability. *Proceedings of the National Academy of Sciences* 106(33):14174–14179.

20. Müller J, et al. (2015) Iron-Dependent Callose Deposition Adjusts Root Meristem Maintenance to Phosphate Availability. *Dev Cell* 33(2):216–230.

21. Iuchi S, et al. (2007) Zinc finger protein STOP1 is critical for proton tolerance in Arabidopsis and coregulates a key gene in aluminum tolerance. *Proc Natl Acad Sci U S A* 104(23):9900–9905.

22. Hoekenga OA, et al. (2006) AtALMT1, which encodes a malate transporter, is identified as one of several genes critical for aluminum tolerance in Arabidopsis. *Proceedings of the National Academy of Sciences* 103(25):9738–9743.

23. Kobayashi Y, et al. (2007) Characterization of AtALMT1 expression in aluminum-inducible malate release and its role for rhizotoxic stress tolerance in Arabidopsis. *Plant Physiol* 145(3):843–852.

24. Colón-Carmona A, You R, Haimovitch-Gal T, Doerner P (1999) Spatio-temporal analysis of mitotic activity with a labile cyclin–GUS fusion protein. *Plant J* 20(4):503–508.

25. Sabatini S, et al. (1999) An auxin-dependent distal organizer of pattern and polarity in the Arabidopsis root. *Cell* 99(5):463–472.

26. Abe A, et al. (2012) Genome sequencing reveals agronomically important loci in rice using MutMap. *Nat Biotechnol* 30(2):174–178.

27. Cingolani P, et al. (2012) A program for annotating and predicting the effects of single nucleotide polymorphisms, SnpEff: SNPs in the genome of Drosophila melanogaster strain w1118; iso-2; iso-3. *Fly* 6(2):80–92.

28. Sawaki Y, et al. (2009) STOP1 regulates multiple genes that protect arabidopsis from proton and aluminum toxicities. *Plant Physiol* 150(1):281–294.

29. Tokizawa M, et al. (2015) SENSITIVE TO PROTON RHIZOTOXICITY1, CALMODULIN BINDING TRANSCRIPTION ACTIVATOR2, and other transcription factors are involved in ALUMINUM-ACTIVATED MALATE TRANSPORTER1 expression. *Plant Physiol* 167(3):991–1003.

30. Jones DL (1998) Organic acids in the rhizosphere – a critical review. *Plant Soil* 205(1):25–44.

31. Grillet L, et al. (2014) Ascorbate efflux as a new strategy for iron reduction and transport in plants. *J Biol Chem* 289(5):2515–2525.

32. Rellán-Alvarez R, et al. (2010) Identification of a tri-iron(III), tri-citrate complex in the xylem sap of iron-deficient tomato resupplied with iron: new insights into plant iron long-distance transport. *Plant Cell Physiol* 51(1):91–102.

33. Ziegler J, et al. (2016) Non-targeted profiling of semi-polar metabolites in Arabidopsis root exudates uncovers a role for coumarin secretion and lignification during the local response to phosphate limitation. *J Exp Bot* 67(5):1421–1432.

34. Puga MI, et al. (2014) SPX1 is a phosphate-dependent inhibitor of PHOSPHATE STARVATION RESPONSE 1 in Arabidopsis. *Proceedings of the National Academy of Sciences* 111(41):14947–14952.

35. Hoehenwarter W, et al. (2016) Comparative expression profiling reveals a role of the root apoplast in local phosphate response. *BMC Plant Biol* 16(1):106.

36. Francoz E, et al. (2015) Roles of cell wall peroxidases in plant development. *Phytochemistry* 112:15–21.

37. Chacón-López A, Ibarra-Laclette E, Sánchez-Calderón L, Gutiérrez-Alanis D, Herrera-Estrella L (2011) Global expression pattern comparison between low phosphorus insensitive 4 and WT Arabidopsis reveals an important role of reactive oxygen species and jasmonic acid in the root tip response to phosphate starvation. *Plant Signal Behav* 6(3):382–392.

38. Tsukagoshi H, Busch W, Benfey PN (2010) Transcriptional regulation of ROS controls transition from proliferation to differentiation in the root. *Cell* 143(4):606–616.

39. Li W, Lan P (2015) Genome-wide analysis of overlapping genes regulated by iron deficiency and phosphate starvation reveals new interactions in Arabidopsis roots. *BMC Res Notes* 8:555.

40. Torabinejad J, Donahue JL, Gunesekera BN, Allen-Daniels MJ, Gillaspy GE (2009) VTC4 is a bifunctional enzyme that affects myoinositol and ascorbate biosynthesis in plants. *Plant Physiol* 150(2):951–961.

41. Wang Z, et al. (2014) Rice SPX1 and SPX2 inhibit phosphate starvation responses through interacting with PHR2 in a phosphate-dependent manner. *Proc Natl Acad Sci U S A* 111(41):14953–14958.

42. Thieme CJ, et al. (2015) Endogenous Arabidopsis messenger RNAs transported to distant tissues. *Nat Plants* 1(4):15025.

43. Kosman DJ (2010) Redox cycling in iron uptake, efflux, and trafficking. *J Biol Chem* 285(35):26729–26735.

44. Luna E, et al. (2011) Callose deposition: a multifaceted plant defense response. *Mol Plant Microbe Interact* 24(2):183–193.

45. Matsuzaki Y, Ogawa-Ohnishi M, Mori A, Matsubayashi Y (2010) Secreted peptide signals required for maintenance of root stem cell niche in Arabidopsis. *Science* 329(5995):1065–1067.

46. Bolger AM, Lohse M, Usadel B (2014) Trimmomatic: a flexible trimmer for Illumina sequence data. *Bioinformatics* 30(15):2114–2120.

47. Li H, Durbin R (2009) Fast and accurate short read alignment with Burrows-Wheeler transform. *Bioinformatics* 25(14):1754–1760.

48. Li H, et al. (2009) The Sequence Alignment/Map format and SAMtools. *Bioinformatics* 25(16):2078–2079.

49. Danecek P, et al. (2011) The variant call format and VCFtools. *Bioinformatics* 27(15):2156–2158.

50. Robinson JT, et al. (2011) Integrative genomics viewer. *Nat Biotechnol* 29(1):24–26.

51. Martinez-Trujillo M, Limones-Briones V, Cabrera-Ponce JL, Herrera-Estrella L (2012) Improving transformation efficiency ofArabidopsis thaliana by modifying the floral dip method. *Plant Mol Biol Rep* 22(1):63–70.

52. Jefferson RA, Kavanagh TA, Bevan MW (1987) GUS fusions: beta-glucuronidase as a sensitive and versatile gene fusion marker in higher plants. *EMBO J* 6(13):3901–3907.

53. Malamy JE, Benfey PN (1997) Organization and cell differentiation in lateral roots of Arabidopsis thaliana. *Development* 124(1):33–44.

54. Li P, Merz KM Jr (2014) Taking into Account the Ion-induced Dipole Interaction in the Nonbonded Model of Ions. *J Chem Theory Comput* 10(1):289–297.

55. Li P, Song LF, Merz KM Jr (2015) Parameterization of highly charged metal ions using the 12-6-4 LJ-type nonbonded model in explicit water. *J Phys Chem B* 119(3):883–895.

56. Bekker H, et al. (1993) PHYSICS COMPUTING '92. *GROMACS - A PARALLEL COMPUTER FOR MOLECULAR-DYNAMICS SIMULATIONS* Available at: http://www.rug.nl/research/portal/publications/gromacs--a-parallel-computer-for-moleculardynamics-simulations(84ef8765-003b-421d-b570-b9c5a3f78a9b).html [Accessed December 16, 2016].

57. Malde AK, et al. (2011) An Automated Force Field Topology Builder (ATB) and Repository: Version 1.0. *J Chem Theory Comput* 7(12):4026–4037.

58. Berendsen HJC, Grigera JR, P. T (1987) The Missing Term in Effective Pair Potentialst. *J Phys Chem* 91:6269–6271.

59. Bussi G, Donadio D, Parrinello M (2007) Canonical sampling through velocity rescaling. *J Chem Phys* 126(1):014101.

60. Essmann U, et al. (1998) A smooth particle mesh Ewald method. *J Chem Phys*. doi:10.1063/1.470117.

61. Darden T, York D, Pedersen L (1998) Particle mesh Ewald: An N·log(N) method for Ewald sums in large systems. *J Chem Phys*. doi:10.1063/1.464397.

62. Hess B, Bekker H, Berendsen HJC, Fraaije JGEM (1997) LINCS: A linear constraint solver for molecular simulations. *J Comput Chem* 18(12):1463–1472.

63. Parrinello M (1981) Polymorphic transitions in single crystals: A new molecular dynamics method. *J Appl Phys* 52(12):7182.

1072 64. Barnoud J, Rossi G, Monticelli L (2014) Lipid membranes as solvents for carbon
1073   nanoparticles. *Phys Rev Lett* 112(6):068102.

1074 65. Yong-Villalobos L, et al. (2015) Methylome analysis reveals an important role for
1075   epigenetic changes in the regulation of the Arabidopsis response to phosphate
1076   starvation. *Proc Natl Acad Sci U S A* 112(52):E7293–302.

1077 66. Kim D, et al. (2013) TopHat2: accurate alignment of transcriptomes in the presence of
1078   insertions, deletions and gene fusions. *Genome Biol* 14(4):R36.

1079 67. Anders S, Pyl PT, Huber W (2015) HTSeq--a Python framework to work with high-
1080   throughput sequencing data. *Bioinformatics* 31(2):166–169.

1081 68. Robinson MD, McCarthy DJ, Smyth GK (2010) edgeR: a Bioconductor package for
1082   differential expression analysis of digital gene expression data. *Bioinformatics*
1083   26(1):139–140.

1084 69. Shannon P, et al. (2003) Cytoscape: a software environment for integrated models of
1085   biomolecular interaction networks. *Genome Res* 13(11):2498–2504.

1086 70. Bindea G, et al. (2009) ClueGO: a Cytoscape plug-in to decipher functionally grouped
1087   gene ontology and pathway annotation networks. *Bioinformatics* 25(8):1091–1093.

1088

1089

1090 **Supplementary Material**

1091

| Cross	F1 progeny		F2 progeny						
	Phenotypes		Phenotype observed		Ration obtained		Ration tested		X^{2*}
	WT	mutant	WT	mutant	WT	mutant	WT	mutant	
lpi5 x Col-0	179	0	490	170	2.97 :	1.03	3 :	1	0.2
lpi6 x Col-0	148	0	577	182	3.04 :	0.96			0.42
							[a]95%		3.841

* With one degree of freedom and a critical value of 5% we fail to reject the hypothesis of a Mendelian ratio of segregation (3:1, WT:mutant) if the x^2 is smaller than 3.841.

1092

1093 **Supplementary Table 1. Segregation ratios of the F2 progeny seedlings obtained**
1094 **from *lpi5* X WT and *lpi6* X WT crosses.**

1095

1096

1097

1098

1099
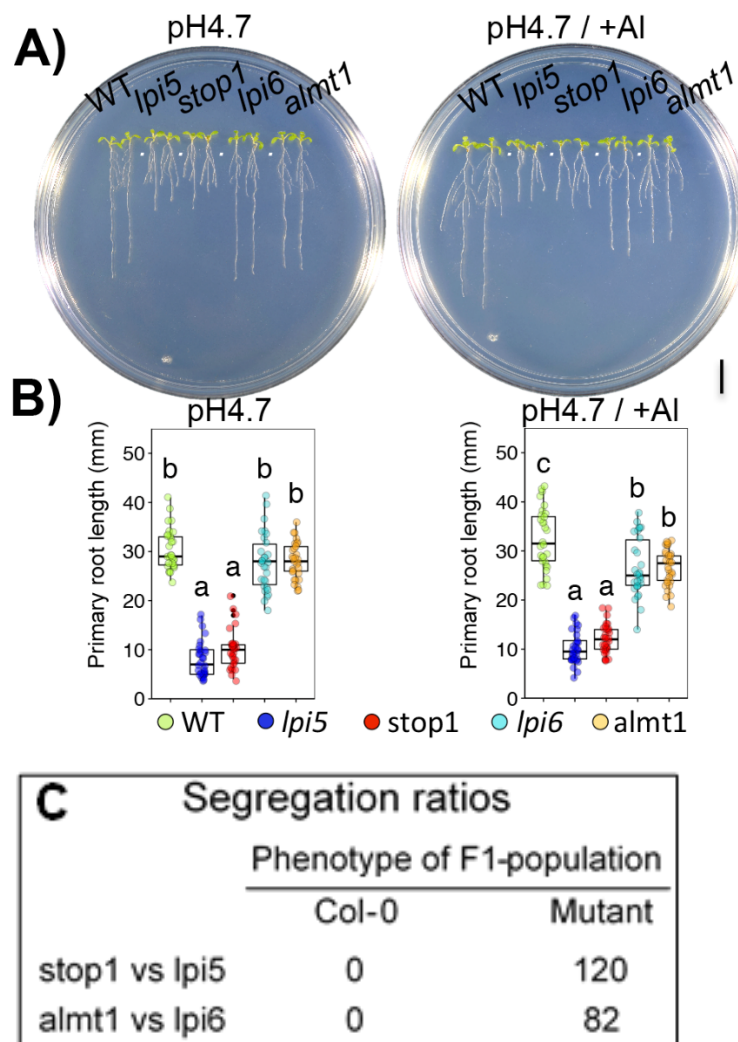
Supplementary Figure 1. **Primary root growth of *lpi5*, *stop1*, *lpi6* and *almt1* 10-day-old seedlings in response to low pH and aluminum toxicity.** (A) Boxplot representation of the primary root length of WT, *lpi5, stop1, lpi6,* and *almt1* 10-day-old individuals (n=30) grown under low pH (4.6) (left) and aluminum toxicity (2 µM) (right) conditions. Dots represent individuals and genetic backgrounds are depicted by colors as described. Statistical groups were determined using a Tukey HSD test (P-value < .05) and are indicated by a letter. B) WT, *lpi5, stop1, lpi6,* and *almt1* 10-dag seedlings grown under low pH (4.6) (left) and aluminum toxicity (2 µM) (right) conditions. Scale bar equals 1 mm. C) Segregation ratios of F1 progeny seedlings (long root phenotype under -Pi conditions) obtained from *stop1* vs *lpi5* and *almt1* vs *lpi6* crosses. All F1 progeny seedlings from the *lpi5* x *salk_114108* and *lpi6* x *salk_009629* crosses were observed to have a mutant phenotype under –Pi conditions.

1114
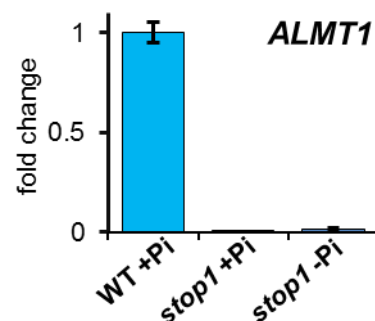
Supplementary Figure 2. *STOP1 is essential for ALMT1 expression in the root tip.* qRT-PCR analysis of *ALMT1* expression in root apex of WT and *stop1* plants. Bars represent the mean logFC ±SEM of 2 biological replicates with 3 technical replicates. WT +Pi samples were used as calibrator values. *ACT2* and *UBQ10* were used as internal controls.


1119
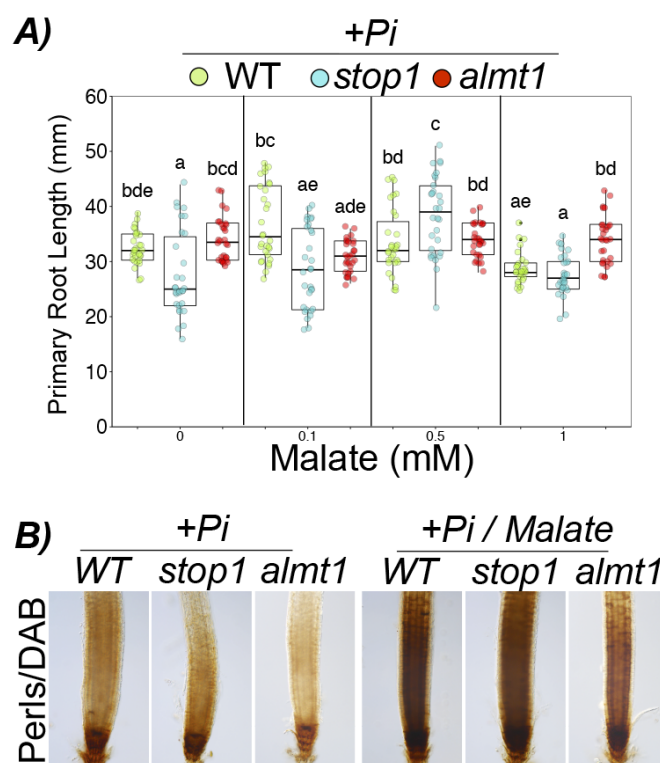
Supplementary Figure 3. Malate effect on primary root growth and iron distribution in the root under high phosphate conditions. (A) Primary root length of 10 dag WT, *stop1* and *almt1* seedlings in response to increasing concentrations of malate supplemented to +Pi medium. (B) DAB-Perls iron staining of roots from 10 dag Col-0, *stop1* and *almt1* seedlings grown under +Pi and +Pi medium supplemented with 1 mM malate (+Pi+M).
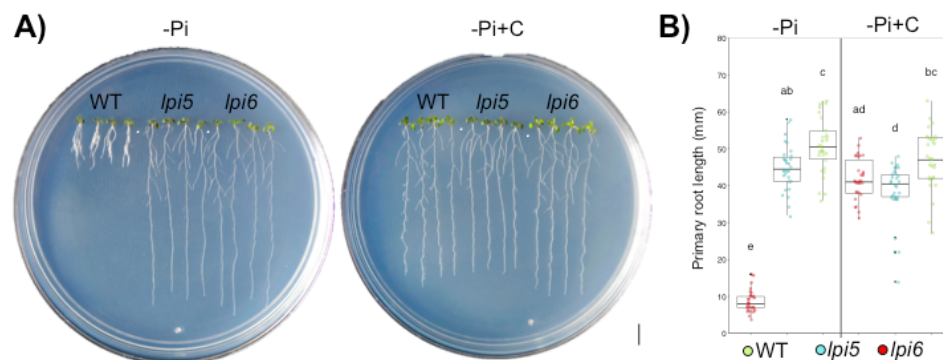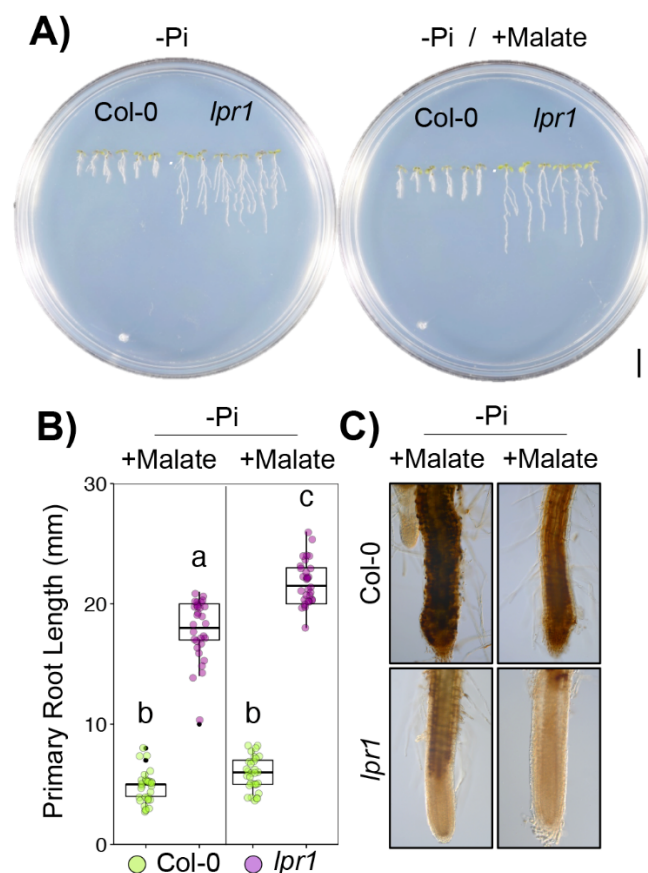
Supplementary Figure 4. Citrate supplementation of low Pi medium did not rescue the long root phenotype of *stop1 and almt1* mutants. (A) Phenotypes of 10 dag WT, *stop1* and *almt1* seedlings grown in low phosphate medium (-Pi) and low phosphate medium supplemented with 1mM citrate (-Pi+C). Scale bar equals 1 mm. (B) Primary root length of 10 dag WT, *stop1* and *almt1* seedlings under -Pi and -Pi medium supplemented with 1mM citrate. Green, blue and red dots depict WT, *stop1* and *almt1* individuals (n=30 from 3 independent experiments), respectively.

1133   Statistical groups were determined using Tukey HSD test (P-value <.05) are indicated with letters.

1134
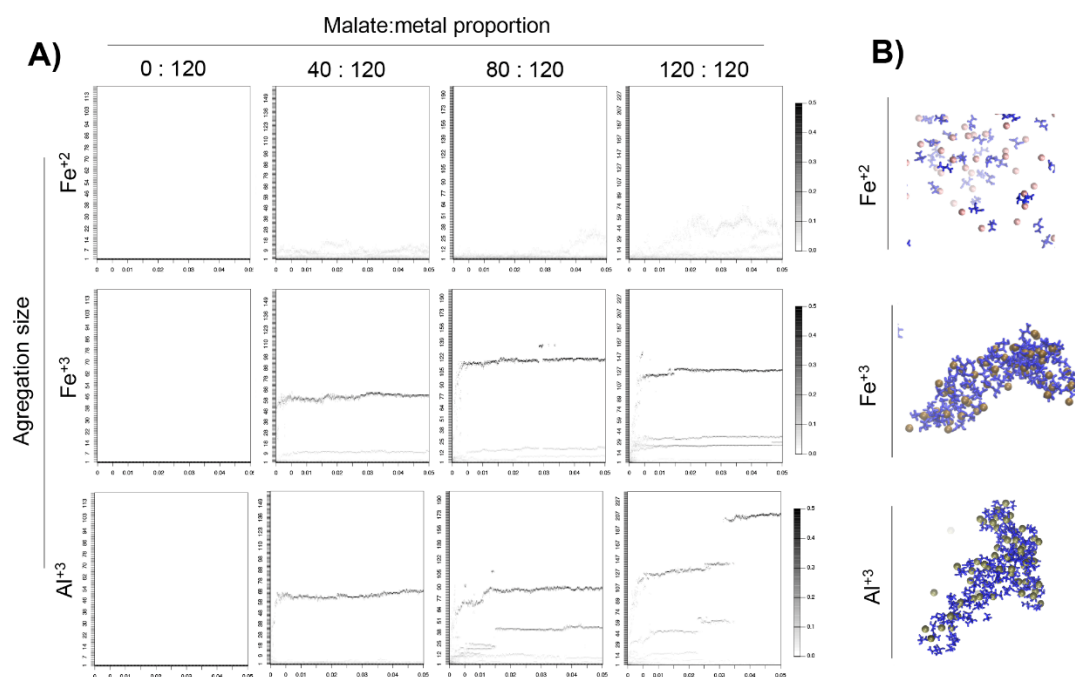
1135   **Supplementary Figure 5. Molecular dynamic calculations revealed the malate-chelating**
1136   **effect that induces Fe³⁺ aggregation.** 120 molecules of each metal (A-D) Fe^{2+}, (E-H) Fe^{3+} and (I-L)
1137   was simulated (see Materials and Methods) with 0, 40, 80 and 100 molecules of malate,
1138   respectively. Structural representation at the end (50 microseconds) of simulation between the
1139   higher malate concentration (120 molecules) and (M) Fe^{2+}, (N) Fe^{3+} and (O) Al^{3+}, respectively.

1140

1141 **Supplementary Figure 6. Malate supplementation of low Pi medium did not rescue the long**
1142 **root phenotype of _lpr1_ mutants.** (A) Phenotypes of Col-0 (WT) and _lpr1_ seedlings grown under
1143 -Pi conditions (left) and -Pi medium supplemented with 1 mM malate (-Pi+M) (right) conditions 10
1144 dag. (B) Primary root length of 10 dag WT and _lpr1_ seedlings grown under -Pi conditions and -Pi+M
1145 conditions. (C) DAB-Perls iron staining of roots from Col-0 and _lpr1_ seedlings grown under -Pi and
1146 -Pi+M conditions 10 dag.

1147

1148

A

atID	logFC repressed / induced					Description
	WT	stop1	stop1 +M	almt1	almt1 +M	
AT5G05340	13.6	2.4	3.6	0.9	7.5	PRX52__Peroxidase superfamily protein
AT2G18150	8.2	3.0	3.8	3.1	6.8	Peroxidase superfamily protein
AT4G36430	8.0	2.9	4.0	2.7	5.1	Peroxidase superfamily protein
AT4G08780	5.9	-0.2	1.5	-0.7	2.5	Peroxidase superfamily protein
AT5G06720	5.4	1.1	2.8	-1.0	2.1	ATPA2_AtPRX53_PA2_PRX53__peroxidase 2
AT5G06730	4.4	0.9	1.8	0.3	2.5	Peroxidase superfamily protein
AT5G39580	4.1	1.2	0.7	1.1	2.9	Peroxidase superfamily protein
AT4G08770	3.3	0.6	3.1	0.4	2.7	Prx37__Peroxidase superfamily protein
AT5G15180	-1.6	-0.7	-3.0	-0.4	-2.2	Peroxidase superfamily protein
AT1G14540	-1.7	-0.2	-2.7	-0.3	-2.1	PER4__Peroxidase superfamily protein
AT2G39040	-2.1	-0.2	-1.6	-0.7	-1.3	Peroxidase superfamily protein
AT3G01190	-2.9	-0.5	-2.2	-0.3	-1.8	Peroxidase superfamily protein

B

atID	WT	stop1	stop1 +M	almt1	almt1 +M	Description
AT1G06490	1.1	0.1	1.1	0.1	0.8	ATGSL07_CalS7_GSL07_GSL7_atgsl7__glucan synthase-like 7
AT3G07160	1.1	0.6	1.2	0.2	1.1	ATGSL10_CALS9_GSL10__glucan synthase-like 10
AT3G14570	1.1	0.5	1.1	0.1	0.5	ATGSL04_GSL04_GSL4_atgsl4__glucan synthase-like 4
AT4G03550	1.1	0.6	1.6	0.2	1.0	ATGSL05_ATGSL5_EED3_GSL05_GSL5_PMR4__glucan synthase-like 5

1149

1150 Supplementary Figure 7. **Malate treatment rescues the expression of peroxidase and callose**
1151 **synthase genes in Pi-deprived *stop1* and *almt1* seedlings**. The locus ID (atID), description and
1152 the expression values (logFC) of (A) *PEROXIDASE* and (B) *CALLOSE SYNTHASE* genes are
1153 presented for Pi-deprived seedlings (WT, *stop1* and *almt1*) and malate-treated Pi-deprived
1154 seedlings (*stop1*+M, *almt1*+M). Non colored values mean that the gene is not differentially
1155 expressed (FDR>.05) in the respective genotype/conditions.

1156

1157
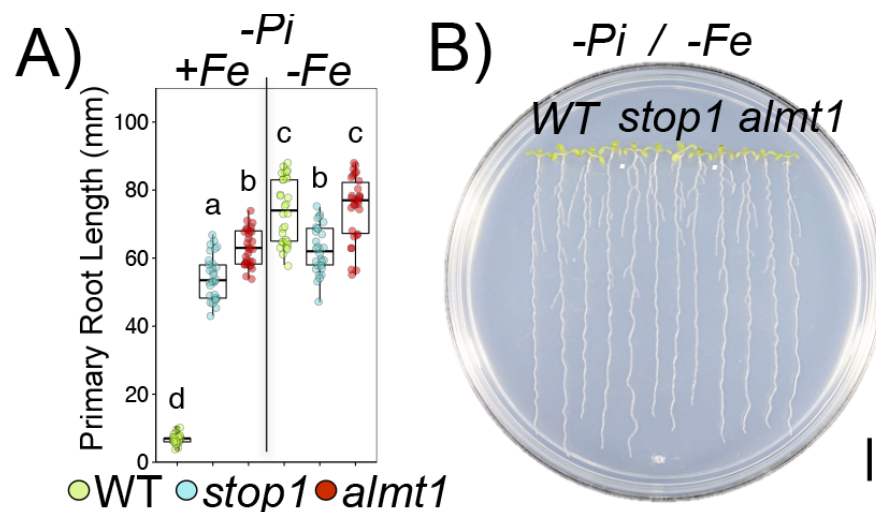
Supplementary Figure 8. Iron-dependence of the inhibition of primary root under low Pi conditions. (A) Primary root length of 10 dag WT, *stop1* and *almt1* seedlings grown In –Pi media (-Pi+Fe) and –Pi media lacking Fe (-Pi-Fe; See Materials and Methods). Green, blue and red dots depict WT, *stop1* and *almt1* individuals (n=30 from 3 independent experiments), respectively. (B) Phenotypes of 10 dag WT, *almt1* and *stop1* seedlings grown under -Pi-Fe conditions. Scale bar equals 1 centimeter (cm).